

Production of $\psi(4040)$, $\psi(4160)$, and $\psi(4415)$ mesons in strong interactions

Sheng-Nan Xu and Xiao-Ming Xu

Department of Physics, Shanghai University, Baoshan, Shanghai 200444, China

Abstract

Using inelastic scattering of charmed strange mesons by open-charm mesons in Pb-Pb collisions at the Large Hadron Collider, we study the production of $\psi(4040)$, $\psi(4160)$, and $\psi(4415)$ mesons. Master rate equations with the inelastic scattering are established. The scattering is caused by quark interchange in association with color interactions between all constituent pairs in different mesons. We consider fifty-one reactions between charmed strange mesons and open-charm mesons. Unpolarized cross sections for the reactions are obtained from a temperature-dependent interquark potential. Temperature dependence of the cross sections leads to that contributions of the reactions to the production of $\psi(4040)$, $\psi(4160)$, and $\psi(4415)$ change with decreasing temperature during evolution of hadronic matter. For central Pb-Pb collisions at $\sqrt{s_{NN}} = 5.02$ TeV it turned out from the master rate equations that the $\psi(4040)$ number density is larger than the $\psi(4160)$ number density which is larger than the $\psi(4415)$ number density.

Keywords: Inelastic meson-meson scattering, quark interchange, relativistic constituent quark potential model, master rate equation.

PACS: 13.75.Lb; 12.39.Jh; 12.39.Pn

I. INTRODUCTION

Since the discovery of $\psi(4040)$, $\psi(4160)$, and $\psi(4415)$ mesons produced in electron-positron collisions [1–3], the three mesons have long been of interest to hadron physi-

cists [4–10]. They are easily produced at electron-positron colliders. Via electromagnetic interactions the electron and the positron become a virtual photon which splits into a charm quark and a charm antiquark. This colorless $c\bar{c}$ pair with a small size evolves into a $c\bar{c}$ meson directly if the $c\bar{c}$ relative momentum is small or indirectly by radiating gluons if the relative momentum is large. The production of $\psi(4040)$, $\psi(4160)$, and $\psi(4415)$ in e^+e^- annihilation can be studied in nonrelativistic quantum chromodynamics that includes color-singlet and color-octet contributions [11] or from an electron-positron-photon vertex, a photon propagator, and direct connection between the photon and the $\psi(4040)$ and $\psi(4160)$ meson fields [12, 13].

Further interest in $\psi(4040)$, $\psi(4160)$, and $\psi(4415)$ mesons has arisen in the context of ultrarelativistic heavy-ion collisions. The history of ultrarelativistic heavy-ion collisions is divided into the following stages: initial nucleus-nucleus collisions, thermalization of deconfined quark-gluon matter that has no temperatures, evolution of quark-gluon plasmas, hadronization of the quark-gluon plasma at the critical temperature T_c , and evolution of hadronic matter until kinetic freeze-out. Some species of hadrons produced in Pb-Pb collisions at the Large Hadron Collider (LHC) have been measured. We expect the production of $\psi(4040)$, $\psi(4160)$, and $\psi(4415)$ mesons in Pb-Pb collisions from quantum chromodynamics (QCD). The $\psi(4040)$, $\psi(4160)$, and $\psi(4415)$ mesons are generally identified with the 3^3S_1 , 2^3D_1 , and 4^3S_1 states of a charm quark and a charm antiquark, respectively [14–17]. Since $\psi(4040)$, $\psi(4160)$, and $\psi(4415)$ mesons are dissolved in hadronic matter when the temperature of hadronic matter is larger than $0.97T_c$, $0.95T_c$, and $0.87T_c$, respectively [18], they can only be produced in hadronic matter. Quark interchange between two open-charm mesons in association with color interactions between two constituents produces the charmonia. Therefore, the production of $\psi(4040)$, $\psi(4160)$, and $\psi(4415)$ can be taken as probes of hadronic matter that results from the quark-gluon plasma created in ultrarelativistic heavy-ion collisions [18].

The production of $\psi(4040)$, $\psi(4160)$, and $\psi(4415)$ mesons in e^+e^- annihilation relates to electromagnetic interactions and strong interactions, while the one in ultrarelativistic heavy-ion collisions only involves strong interactions. The mechanism of the latter is

different from the mechanism of the former. Models corresponding to different mechanisms are different.

Hadronic matter contains not only charmed mesons but also charmed strange mesons. In the present work we study the production of $\psi(4040)$, $\psi(4160)$, and $\psi(4415)$ via quark interchange between a charmed meson and a charmed strange meson and between two charmed strange mesons in hadronic matter. This includes establishing master rate equations with new source terms that involve charmed strange mesons, calculating cross sections for the production of the charmonia in meson scattering by charmed strange mesons, and studying number densities of the charmonia yielded in central Pb-Pb collisions at the center-of-mass energy per nucleon-nucleon pair $\sqrt{s_{NN}} = 5.02$ TeV at the LHC. We note that the charmonium production in scattering of charmed strange mesons by open-charm mesons has not been studied.

In vacuum it is observed that $\psi(4040)$, $\psi(4160)$, and $\psi(4415)$ mesons decay to two open-charm mesons. In hadronic matter D , D^* , D_s , D_s^* , $\psi(4040)$, $\psi(4160)$, and $\psi(4415)$ masses decrease with increasing temperature [18], and the masses of the three charmonia become smaller than the sum of the masses of the two open-charm mesons. The charmonium decays to the two open-charm mesons are forbidden by energy conservation. Hence, the $\psi(4040)$, $\psi(4160)$, and $\psi(4415)$ mesons are stable in hadronic matter.

This paper is organized as follows. In Sect. II we establish master rate equations for $\psi(4040)$, $\psi(4160)$, and $\psi(4415)$ mesons. In Sect. III we provide cross-section formulas for inelastic meson-meson scattering governed by quark interchange. In Sect. IV we exhibit numerical cross sections for twenty-seven reactions, show number densities of the three mesons produced in central Pb-Pb collisions, and give relevant discussions. In Sect. V we summarize the present work.

II. MASTER RATE EQUATIONS

We use the notation $D = \begin{pmatrix} D^+ \\ D^0 \end{pmatrix}$, $\bar{D} = \begin{pmatrix} \bar{D}^0 \\ D^- \end{pmatrix}$, $K = \begin{pmatrix} K^+ \\ K^0 \end{pmatrix}$, $\bar{K} = \begin{pmatrix} \bar{K}^0 \\ K^- \end{pmatrix}$,

$D^* = \begin{pmatrix} D^{*+} \\ D^{*0} \end{pmatrix}$, $\bar{D}^* = \begin{pmatrix} \bar{D}^{*0} \\ D^{*-} \end{pmatrix}$, $K^* = \begin{pmatrix} K^{*+} \\ K^{*0} \end{pmatrix}$, and $\bar{K}^* = \begin{pmatrix} \bar{K}^{*0} \\ K^{*-} \end{pmatrix}$ for the isospin doublets. Hadronic matter produced in Pb-Pb collisions at LHC energies contain many charmed mesons and charmed strange mesons. The production of $\psi(4040)$, $\psi(4160)$, and $\psi(4415)$ mesons from two charmed mesons has been studied in Ref. [19]. Now we consider the production of $\psi(4040)$, $\psi(4160)$, and $\psi(4415)$ from a charmed strange meson and a charmed meson and from two charmed strange mesons as follows:

$$\begin{aligned}
D_s^+ \bar{D} &\rightarrow K^* \psi(4040), \quad D_s^+ \bar{D} \rightarrow K^* \psi(4160), \quad D_s^+ \bar{D} \rightarrow K^* \psi(4415), \\
D_s^+ \bar{D}^* &\rightarrow K \psi(4040), \quad D_s^+ \bar{D}^* \rightarrow K \psi(4160), \quad D_s^+ \bar{D}^* \rightarrow K \psi(4415), \\
D_s^+ \bar{D}^* &\rightarrow K^* \psi(4040), \quad D_s^+ \bar{D}^* \rightarrow K^* \psi(4160), \quad D_s^+ \bar{D}^* \rightarrow K^* \psi(4415), \\
D_s^{*+} \bar{D} &\rightarrow K \psi(4040), \quad D_s^{*+} \bar{D} \rightarrow K \psi(4160), \quad D_s^{*+} \bar{D} \rightarrow K \psi(4415), \\
D_s^{*+} \bar{D} &\rightarrow K^* \psi(4040), \quad D_s^{*+} \bar{D} \rightarrow K^* \psi(4160), \quad D_s^{*+} \bar{D} \rightarrow K^* \psi(4415), \\
D_s^{*+} \bar{D}^* &\rightarrow K \psi(4040), \quad D_s^{*+} \bar{D}^* \rightarrow K \psi(4160), \quad D_s^{*+} \bar{D}^* \rightarrow K \psi(4415), \\
D_s^{*+} \bar{D}^* &\rightarrow K^* \psi(4040), \quad D_s^{*+} \bar{D}^* \rightarrow K^* \psi(4160), \quad D_s^{*+} \bar{D}^* \rightarrow K^* \psi(4415), \\
D_s^+ D_s^{*-} &\rightarrow \eta \psi(4040), \quad D_s^+ D_s^{*-} \rightarrow \eta \psi(4160), \quad D_s^+ D_s^{*-} \rightarrow \eta \psi(4415), \\
D_s^{*+} D_s^{*-} &\rightarrow \eta \psi(4040), \quad D_s^{*+} D_s^{*-} \rightarrow \eta \psi(4160), \quad D_s^{*+} D_s^{*-} \rightarrow \eta \psi(4415).
\end{aligned}$$

Applying charge conjugation to the above reactions, we obtain $D_s^- D$, $D_s^- D^*$, $D_s^{*-} D$, $D_s^{*-} D^*$, and $D_s^- D_s^{*+}$ reactions.

Denote the number densities of $\psi(4040)$, $\psi(4160)$, and $\psi(4415)$ mesons by $n_{\psi(4040)}$, $n_{\psi(4160)}$, and $n_{\psi(4415)}$, respectively. These number densities change according to the following rate equations,

$$\partial_\mu (n_R u^\mu) = \Theta_R, \tag{1}$$

where μ is the space-time index, R stands for $\psi(4040)$, $\psi(4160)$, or $\psi(4415)$, and u^μ is the four-velocity of a fluid element in hadronic matter. Denote by v_{ij} the relative velocity of

mesons i and j , and by $\sigma_{ij \rightarrow i'j'}$ the isospin-averaged unpolarized cross section for $ij \rightarrow i'j'$.

The source terms are given by

$$\begin{aligned}
\Theta_R = & \langle \sigma_{D\bar{D} \rightarrow \rho R} v_{D\bar{D}} \rangle n_D n_{\bar{D}} + \langle \sigma_{D\bar{D}^* \rightarrow \pi R} v_{D\bar{D}^*} \rangle n_D n_{\bar{D}^*} \\
& + \langle \sigma_{D^* \bar{D} \rightarrow \pi R} v_{D^* \bar{D}} \rangle n_{D^*} n_{\bar{D}} + \langle \sigma_{D\bar{D}^* \rightarrow \rho R} v_{D\bar{D}^*} \rangle n_D n_{\bar{D}^*} \\
& + \langle \sigma_{D^* \bar{D} \rightarrow \rho R} v_{D^* \bar{D}} \rangle n_{D^*} n_{\bar{D}} + \langle \sigma_{D^* \bar{D}^* \rightarrow \pi R} v_{D^* \bar{D}^*} \rangle n_{D^*} n_{\bar{D}^*} \\
& + \langle \sigma_{D^* \bar{D}^* \rightarrow \rho R} v_{D^* \bar{D}^*} \rangle n_{D^*} n_{\bar{D}^*} + \langle \sigma_{D_s^+ \bar{D} \rightarrow K^* R} v_{D_s^+ \bar{D}} \rangle n_{D_s^+} n_{\bar{D}} \\
& + \langle \sigma_{D_s^- D \rightarrow \bar{K}^* R} v_{D_s^- D} \rangle n_{D_s^-} n_D + \langle \sigma_{D_s^+ \bar{D}^* \rightarrow K R} v_{D_s^+ \bar{D}^*} \rangle n_{D_s^+} n_{\bar{D}^*} \\
& + \langle \sigma_{D_s^- D^* \rightarrow \bar{K} R} v_{D_s^- D^*} \rangle n_{D_s^-} n_{D^*} + \langle \sigma_{D_s^+ \bar{D}^* \rightarrow K^* R} v_{D_s^+ \bar{D}^*} \rangle n_{D_s^+} n_{\bar{D}^*} \\
& + \langle \sigma_{D_s^- D^* \rightarrow \bar{K}^* R} v_{D_s^- D^*} \rangle n_{D_s^-} n_{D^*} + \langle \sigma_{D_s^{*+} \bar{D} \rightarrow K R} v_{D_s^{*+} \bar{D}} \rangle n_{D_s^{*+}} n_{\bar{D}} \\
& + \langle \sigma_{D_s^{*-} D \rightarrow \bar{K} R} v_{D_s^{*-} D} \rangle n_{D_s^{*-}} n_D + \langle \sigma_{D_s^{*+} \bar{D} \rightarrow K^* R} v_{D_s^{*+} \bar{D}} \rangle n_{D_s^{*+}} n_{\bar{D}} \\
& + \langle \sigma_{D_s^{*-} D \rightarrow \bar{K}^* R} v_{D_s^{*-} D} \rangle n_{D_s^{*-}} n_D + \langle \sigma_{D_s^{*+} \bar{D}^* \rightarrow K R} v_{D_s^{*+} \bar{D}^*} \rangle n_{D_s^{*+}} n_{\bar{D}^*} \\
& + \langle \sigma_{D_s^{*-} D^* \rightarrow \bar{K} R} v_{D_s^{*-} D^*} \rangle n_{D_s^{*-}} n_{D^*} + \langle \sigma_{D_s^{*+} \bar{D}^* \rightarrow K^* R} v_{D_s^{*+} \bar{D}^*} \rangle n_{D_s^{*+}} n_{\bar{D}^*} \\
& + \langle \sigma_{D_s^{*-} D^* \rightarrow \bar{K}^* R} v_{D_s^{*-} D^*} \rangle n_{D_s^{*-}} n_{D^*} + \langle \sigma_{D_s^+ D_s^{*-} \rightarrow \eta R} v_{D_s^+ D_s^{*-}} \rangle n_{D_s^+} n_{D_s^{*-}} \\
& + \langle \sigma_{D_s^{*+} D_s^- \rightarrow \eta R} v_{D_s^{*+} D_s^-} \rangle n_{D_s^{*+}} n_{D_s^-} + \langle \sigma_{D_s^{*+} D_s^{*-} \rightarrow \eta R} v_{D_s^{*+} D_s^{*-}} \rangle n_{D_s^{*+}} n_{D_s^{*-}} \\
& - \langle \sigma_{\rho R \rightarrow D\bar{D}} v_{\rho R} \rangle n_\rho n_R - \langle \sigma_{\pi R \rightarrow D\bar{D}^*} v_{\pi R} \rangle n_\pi n_R \\
& - \langle \sigma_{\pi R \rightarrow D^* \bar{D}} v_{\pi R} \rangle n_\pi n_R - \langle \sigma_{\rho R \rightarrow D\bar{D}^*} v_{\rho R} \rangle n_\rho n_R \\
& - \langle \sigma_{\rho R \rightarrow D^* \bar{D}} v_{\rho R} \rangle n_\rho n_R - \langle \sigma_{\pi R \rightarrow D^* \bar{D}^*} v_{\pi R} \rangle n_\pi n_R \\
& - \langle \sigma_{\rho R \rightarrow D^* \bar{D}^*} v_{\rho R} \rangle n_\rho n_R - \langle \sigma_{K^* R \rightarrow D_s^+ \bar{D}} v_{K^* R} \rangle n_{K^*} n_R \\
& - \langle \sigma_{\bar{K}^* R \rightarrow D_s^- D} v_{\bar{K}^* R} \rangle n_{\bar{K}^*} n_R - \langle \sigma_{K R \rightarrow D_s^+ \bar{D}^*} v_{K R} \rangle n_K n_R \\
& - \langle \sigma_{\bar{K} R \rightarrow D_s^- D^*} v_{\bar{K} R} \rangle n_{\bar{K}} n_R - \langle \sigma_{K^* R \rightarrow D_s^+ \bar{D}^*} v_{K^* R} \rangle n_{K^*} n_R \\
& - \langle \sigma_{\bar{K}^* R \rightarrow D_s^- D^*} v_{\bar{K}^* R} \rangle n_{\bar{K}^*} n_R - \langle \sigma_{K R \rightarrow D_s^+ \bar{D}} v_{K R} \rangle n_K n_R \\
& - \langle \sigma_{\bar{K} R \rightarrow D_s^- D^*} v_{\bar{K} R} \rangle n_{\bar{K}} n_R - \langle \sigma_{K^* R \rightarrow D_s^+ \bar{D}^*} v_{K^* R} \rangle n_{K^*} n_R \\
& - \langle \sigma_{\bar{K}^* R \rightarrow D_s^{*-} D} v_{\bar{K}^* R} \rangle n_{\bar{K}^*} n_R - \langle \sigma_{K R \rightarrow D_s^+ \bar{D}^*} v_{K R} \rangle n_K n_R \\
& - \langle \sigma_{\bar{K} R \rightarrow D_s^{*-} D^*} v_{\bar{K} R} \rangle n_{\bar{K}} n_R - \langle \sigma_{K^* R \rightarrow D_s^+ \bar{D}^*} v_{K^* R} \rangle n_{K^*} n_R \\
& - \langle \sigma_{\bar{K}^* R \rightarrow D_s^{*-} D^*} v_{\bar{K}^* R} \rangle n_{\bar{K}^*} n_R - \langle \sigma_{\eta R \rightarrow D_s^+ D_s^{*-}} v_{\eta R} \rangle n_\eta n_R \\
& - \langle \sigma_{\eta R \rightarrow R D_s^+ D_s^-} v_{\eta R} \rangle n_\eta n_R - \langle \sigma_{\eta R \rightarrow D_s^+ D_s^{*-}} v_{\eta R} \rangle n_\eta n_R,
\end{aligned}$$

(2)

where $n_D, n_{\bar{D}}, n_{D^*}, n_{\bar{D}^*}, n_{D_s^+}, n_{D_s^-}, n_{D_s^{*+}}, n_{D_s^{*-}}, n_\pi, n_\rho, n_K, n_{\bar{K}}, n_{K^*}, n_{\bar{K}^*}$, and n_η are the number densities of $D, \bar{D}, D^*, \bar{D}^*, D_s^+, D_s^-, D_s^{*+}, D_s^{*-}, \pi, \rho, K, \bar{K}, K^*, \bar{K}^*$, and η mesons, respectively; $\langle \sigma_{ij \rightarrow i'j'} v_{ij} \rangle$ indicates the average cross section weighted by the relative velocity,

$$\langle \sigma_{ij \rightarrow i'j'} v_{ij} \rangle = \frac{\int \frac{d^3 k_i}{(2\pi)^3} f_i(k_i) \frac{d^3 k_j}{(2\pi)^3} f_j(k_j) \sigma_{ij \rightarrow i'j'}(\sqrt{s}, T) v_{ij}}{\int \frac{d^3 k_i}{(2\pi)^3} f_i(k_i) \int \frac{d^3 k_j}{(2\pi)^3} f_j(k_j)}, \quad (3)$$

where \sqrt{s} is the center-of-mass energy of mesons i and j , T the temperature, and $f_i(k_i)$ the momentum distribution function of meson i with the four-momentum k_i in the rest frame of hadronic matter. The first seven terms on the right-hand side of Eq. (2) have been taken into account in Ref. [19]. While the first twenty-four terms produce $\psi(4040)$, $\psi(4160)$, and $\psi(4415)$ mesons, the last twenty-four terms break them.

The master rate equations involve the temperature and the transverse velocity of hadronic matter, which are given by the relativistic hydrodynamic equation,

$$\partial_\mu T^{\mu\nu} = 0, \quad (4)$$

where $T^{\mu\nu}$ is the energy-momentum tensor,

$$T^{\mu\nu} = (\epsilon + P)u^\mu u^\nu - P g^{\mu\nu} + \eta[\nabla^\mu u^\nu + \nabla^\nu u^\mu - \frac{2}{3}(g^{\mu\nu} - u^\mu u^\nu)\nabla \cdot u], \quad (5)$$

where $\nabla^\mu = \partial^\mu - u^\mu u \cdot \partial$; $\epsilon, P, g^{\mu\nu}$, and η are the energy density, the pressure, the metric, and the shear viscosity, respectively.

For a large volume of particles, if cross sections for particle-particle scattering are very large, the mean free path of particles is very short, and matter that the particles form is a perfect fluid [20, 21]. Then, the first two terms on the right-hand side of Eq. (5) give the hydrodynamic equation,

$$\partial_\mu [(\epsilon + P)u^\mu u^\nu - P g^{\mu\nu}] = 0. \quad (6)$$

If the cross sections are not very large, this matter is not a perfect fluid. Then, viscosities such as the shear viscosity, which is proportional to the inverse of the cross sections, need

to be taken into account in studying matter evolution. Influence of the bulk viscosity may be neglected [22]. Including the shear viscosity in the energy-momentum tensor as seen in Eq. (5), Eq. (4) is established [20].

III. CROSS-SECTION FORMULAS

A meson consists of the charm quark c and the light antiquark \bar{q}_2 , and another meson consists of the light quark q_1 and the charm antiquark \bar{c} . When the two mesons collide, interchange of the c quark and the q_1 quark leads to the reaction $c\bar{q}_2 + q_1\bar{c} \rightarrow q_1\bar{q}_2 + c\bar{c}$. We denote the mass and the four-momentum of meson i ($i = c\bar{q}_2, q_1\bar{c}, q_1\bar{q}_2, c\bar{c}$) by m_i and $P_i = (E_i, \vec{P}_i)$, respectively. The Mandelstam variable is $s = (P_{c\bar{q}_2} + P_{q_1\bar{c}})^2$. The unpolarized cross section for $c\bar{q}_2 + q_1\bar{c} \rightarrow q_1\bar{q}_2 + c\bar{c}$ is

$$\sigma^{\text{unpol}}(\sqrt{s}, T) = \frac{1}{(2J_{c\bar{q}_2} + 1)(2J_{q_1\bar{c}} + 1)} \frac{1}{64\pi s} \frac{|\vec{P}'(\sqrt{s})|}{|\vec{P}(\sqrt{s})|} \int_0^\pi d\theta \sum_{J_{c\bar{q}_2 z} J_{q_1\bar{c} z} J_{q_1\bar{q}_2 z} J_{c\bar{c} z}} (|\mathcal{M}_{\text{fi}}^{\text{prior}}|^2 + |\mathcal{M}_{\text{fi}}^{\text{post}}|^2) \sin \theta, \quad (7)$$

where $J_{c\bar{q}_2 z}$ ($J_{q_1\bar{c} z}$, $J_{q_1\bar{q}_2 z}$, $J_{c\bar{c} z}$) denotes the magnetic projection quantum number of the total angular momentum $J_{c\bar{q}_2}$ ($J_{q_1\bar{c}}$, $J_{q_1\bar{q}_2}$, $J_{c\bar{c}}$) of meson $c\bar{q}_2$ ($q_1\bar{c}$, $q_1\bar{q}_2$, $c\bar{c}$); \vec{P} equals $\vec{P}_{c\bar{q}_2}$, and \vec{P}' equals $\vec{P}_{q_1\bar{q}_2}$; θ is the angle between \vec{P} and \vec{P}' .

Quark interchange brings about two forms in the Born-order meson-meson scattering, the prior form and the post form [23, 24]. Scattering in the prior form means that gluon exchange takes place prior to quark interchange. The transition amplitude for scattering in the prior form is

$$\mathcal{M}_{\text{fi}}^{\text{prior}} = 4\sqrt{E_{c\bar{q}_2} E_{q_1\bar{c}} E_{q_1\bar{q}_2} E_{c\bar{c}}} \langle \psi_{q_1\bar{q}_2} | \langle \psi_{c\bar{c}} | (V_{c\bar{c}} + V_{\bar{q}_2 q_1} + V_{c q_1} + V_{\bar{q}_2 \bar{c}}) | \psi_{c\bar{q}_2} \rangle | \psi_{q_1\bar{c}} \rangle, \quad (8)$$

where $\psi_{c\bar{q}_2}$ ($\psi_{q_1\bar{c}}$, $\psi_{q_1\bar{q}_2}$, $\psi_{c\bar{c}}$) is the wave function of meson $c\bar{q}_2$ ($q_1\bar{c}$, $q_1\bar{q}_2$, $c\bar{c}$), and is the product of the color wave function, the spin wave function, the flavor wave function, and the mesonic quark-antiquark relative-motion wave function; V_{ab} is the potential between constituents a and b . Scattering in the post form means that quark interchange is followed

by gluon exchange. The transition amplitude for scattering in the post form is

$$\mathcal{M}_{\text{fi}}^{\text{post}} = 4\sqrt{E_{c\bar{q}_2}E_{q_1\bar{c}}E_{q_1\bar{q}_2}E_{c\bar{c}}} \langle \psi_{q_1\bar{q}_2} | \langle \psi_{c\bar{c}} | (V_{q_1\bar{c}} + V_{\bar{q}_2c} + V_{cq_1} + V_{\bar{q}_2\bar{c}}) | \psi_{c\bar{q}_2} \rangle | \psi_{q_1\bar{c}} \rangle . \quad (9)$$

Both $\mathcal{M}_{\text{fi}}^{\text{prior}}$ and $\mathcal{M}_{\text{fi}}^{\text{post}}$ contain V_{cq_1} and $V_{\bar{q}_2\bar{c}}$. However, it is possible that $\langle \psi_{q_1\bar{q}_2} | \langle \psi_{c\bar{c}} | (V_{c\bar{c}} + V_{\bar{q}_2q_1}) | \psi_{c\bar{q}_2} \rangle | \psi_{q_1\bar{c}} \rangle$ in $\mathcal{M}_{\text{fi}}^{\text{prior}}$ is not the same as $\langle \psi_{q_1\bar{q}_2} | \langle \psi_{c\bar{c}} | (V_{q_1\bar{c}} + V_{\bar{q}_2c}) | \psi_{c\bar{q}_2} \rangle | \psi_{q_1\bar{c}} \rangle$ in $\mathcal{M}_{\text{fi}}^{\text{post}}$. Hence, $\mathcal{M}_{\text{fi}}^{\text{post}}$ may not equal $\mathcal{M}_{\text{fi}}^{\text{prior}}$, which is the so-called post-prior discrepancy [25–27].

The transition amplitudes come from interactions between all constituent pairs in different mesons. In the present work we consider a central spin-independent potential, a spin-spin interaction, and a tensor interaction. Derived from perturbative QCD and lattice gauge calculations [28–30], the potential for $T < T_c$ is,

$$\begin{aligned} V_{ab}(\vec{r}_{ab}) = & -\frac{\vec{\lambda}_a}{2} \cdot \frac{\vec{\lambda}_b}{2} \xi_1 \left[1.3 - \left(\frac{T}{T_c} \right)^4 \right] \tanh(\xi_2 r_{ab}) + \frac{\vec{\lambda}_a}{2} \cdot \frac{\vec{\lambda}_b}{2} \frac{6\pi}{25} \frac{v(\lambda r_{ab})}{r_{ab}} \exp(-\xi_3 r_{ab}) \\ & - \frac{\vec{\lambda}_a}{2} \cdot \frac{\vec{\lambda}_b}{2} \frac{16\pi^2}{25} \frac{d^3}{\pi^{3/2}} \exp(-d^2 r_{ab}^2) \frac{\vec{s}_a \cdot \vec{s}_b}{m_a m_b} + \frac{\vec{\lambda}_a}{2} \cdot \frac{\vec{\lambda}_b}{2} \frac{4\pi}{25} \frac{1}{r_{ab}} \frac{d^2 v(\lambda r_{ab})}{dr_{ab}^2} \frac{\vec{s}_a \cdot \vec{s}_b}{m_a m_b} \\ & - \frac{\vec{\lambda}_a}{2} \cdot \frac{\vec{\lambda}_b}{2} \frac{6\pi}{25 m_a m_b} \left[v(\lambda r_{ab}) - r_{ab} \frac{dv(\lambda r_{ab})}{dr_{ab}} + \frac{r_{ab}^2}{3} \frac{d^2 v(\lambda r_{ab})}{dr_{ab}^2} \right] \\ & \left(\frac{3\vec{s}_a \cdot \vec{r}_{ab} \vec{s}_b \cdot \vec{r}_{ab}}{r_{ab}^5} - \frac{\vec{s}_a \cdot \vec{s}_b}{r_{ab}^3} \right), \end{aligned} \quad (10)$$

where \vec{r}_{ab} is the relative coordinate of constituents a and b ; m_a , \vec{s}_a , and $\vec{\lambda}_a$ are the mass, the spin, and the Gell-Mann matrices for the color generators of constituent a , respectively; $\xi_1 = 0.525$ GeV, $\xi_2 = 1.5[0.75 + 0.25(T/T_c)^{10}]^6$ GeV, $\xi_3 = 0.6$ GeV, $T_c = 0.175$ GeV, and $\lambda = \sqrt{25/16\pi^2\alpha'}$ with $\alpha' = 1.04$ GeV⁻²; the function v is given by Buchmüller and Tye [28]; the quantity d is related to constituent masses [19]. The constituent masses are 0.32 GeV, 0.32 GeV, 0.5 GeV, and 1.51 GeV for the up quark, the down quark, the strange quark, and the charm quark, respectively. The Schrödinger equation with $V_{ab}(\vec{r}_{ab})$ at zero temperature gives meson masses that are close to the experimental masses [31] of π , ρ , K , K^* , J/ψ , χ_c , ψ' , $\psi(3770)$, $\psi(4040)$, $\psi(4160)$, $\psi(4415)$, D , D^* , D_s , and D_s^* mesons. With the mesonic quark-antiquark relative-motion wave functions determined by the Schrödinger equation, the experimental data [32–44] of S - and P -wave elastic phase

shifts for $\pi\pi$ scattering in vacuum are reproduced in the Born approximation [45, 46].

Including color screening in medium, the lattice gauge calculations [29] provide a numerical spin-independent and temperature-dependent potential at intermediate and large distances. The first and second terms on the right-hand side of Eq. (10) fit well the numerical quark potential at $T > 0.55T_c$ [47]. The expression $\frac{\bar{\lambda}_a}{2} \cdot \frac{\bar{\lambda}_b}{2} \frac{6\pi}{25} \frac{v(\lambda r_{ab})}{r_{ab}}$ in the second term arises from one-gluon exchange plus perturbative one- and two-loop corrections in vacuum [28], and the factor $\exp(-\xi_3 r_{ab})$ is a medium modification factor. When the distance increases from zero, the numerical potential increases, and obviously becomes a distance-independent value at large distances at $T > 0.55T_c$. The value decreases with increasing temperature, which means that confinement becomes weaker and weaker. The value is parametrized as $-\frac{\bar{\lambda}_a}{2} \cdot \frac{\bar{\lambda}_b}{2} \xi_1 \left[1.3 - \left(\frac{T}{T_c} \right)^4 \right]$. The function $\tanh(\xi_2 r_{ab})$ increases from 0 to 1 when r_{ab} increases from 0 to $+\infty$. ξ_2 increases when T increases. The larger is ξ_2 , the smaller is the distance at which $\tanh(\xi_2 r_{ab})$ is nearly 1, i.e., the stronger is the medium screening on the quark potential. The first term is the confining potential that corresponds to the lattice results. The third term is the smeared spin-spin interaction that comes from one-gluon exchange between constituents a and b . The fourth term is the spin-spin interaction that originates from perturbative one- and two-loop corrections to one-gluon exchange. The fifth term is the tensor interaction that arises from one-gluon exchange plus perturbative one- and two-loop corrections.

IV. NUMERICAL RESULTS AND DISCUSSIONS

We solve the Schrödinger equation with the potential given in Eq. (10) to obtain temperature-dependent meson masses and mesonic quark-antiquark relative-motion wave functions in coordinate space. Transition amplitudes in the prior form and in the post form are calculated from the Fourier transform of the potential and the wave functions. Temperature-dependent unpolarized cross sections are obtained from Eq. (7). The cross sections are plotted in Figs. 1-27 for the twenty-seven reactions listed in Section II. The cross sections for $D_s^- D$, $D_s^- D^*$, $D_s^{*-} D$, $D_s^{*-} D^*$, and $D_s^- D_s^{*+}$ reactions equal those for $D_s^+ \bar{D}$, $D_s^+ \bar{D}^*$, $D_s^{*+} \bar{D}$, $D_s^{*+} \bar{D}^*$, and $D_s^+ D_s^{*-}$ reactions, respectively. These unpolarized

cross sections lead to the isospin-averaged unpolarized cross sections in the source terms by a formula given in the appendix of Ref. [19].

If the sum of the masses of the two initial mesons of a reaction is smaller than that of the two final mesons, the reaction is endothermic. The threshold energy is the sum of the masses of the two final mesons. At threshold, $|\vec{P}| \neq 0$, $|\vec{P}'| = 0$, and $\sigma^{\text{unpol}} = 0$. Given a temperature, every endothermic reaction has at least a peak cross section. The initial mesons need kinetic energies to satisfy energy conservation and to start the reaction, and a certain amount of the kinetic energies are converted into the masses of the final mesons. If the sum of the masses of the two initial mesons is larger than that of the two final mesons, the reaction is exothermic. The threshold energy is the sum of the masses of the two initial mesons. At threshold, $|\vec{P}| = 0$, $|\vec{P}'| \neq 0$, and $\sigma^{\text{unpol}} = +\infty$. Even slowly-moving initial mesons may start the reaction, and a certain amount of the masses of the initial mesons are converted into kinetic energies of the final mesons. Since meson masses decrease with increasing temperature, the sum of the masses of the two initial mesons may be smaller than the one of the two final mesons at a temperature, but may be larger than the one of the two final mesons at another temperature. Therefore, a reaction may be endothermic at a temperature and exothermic at another temperature.

The Schrödinger equation with the potential given in Eq. (10) yields energy eigenvalues and quark-antiquark relative-motion wave functions in coordinate space. The sum of the quark mass, the antiquark mass, and an eigenvalue gives a meson mass. Since the potential decreases with increasing temperature, eigenvalues and meson masses decrease [18]. Threshold energies which are the sum of the masses of the two final (initial) mesons for endothermic (exothermic) reactions decrease with increasing temperature as seen in Figs. 1-27. Regarding different mesons, reduced amounts of meson masses are different. For example, from $T = 0$ to $T = 0.85T_c$ the K^* and $\psi(4040)$ masses are reduced by 0.399 GeV and 0.859 GeV, respectively, and the threshold energy of $D_s^+ \bar{D} \rightarrow K^* \psi(4040)$ is reduced by 1.258 GeV.

When \sqrt{s} increases from the threshold energy, $|\vec{P}|$ of any endothermic reaction increases from a nonzero value, $|\vec{P}'|$ increases from zero, and $|\vec{P}'| / |\vec{P}|$ causes a rapid

increase of the cross section close to the threshold energy. Since every mesonic quark-antiquark relative momentum is a linear combination of \vec{P} and \vec{P}' , its absolute value increases with increasing \sqrt{s} . Since the mesonic quark-antiquark relative-motion wave functions are decreasing functions of the relative momenta, the transition amplitudes decrease rapidly with increasing \sqrt{s} . The rising $|\vec{P}'| / |\vec{P}|$ and falling transition amplitudes produce a narrow peak in the cross section near the threshold energy.

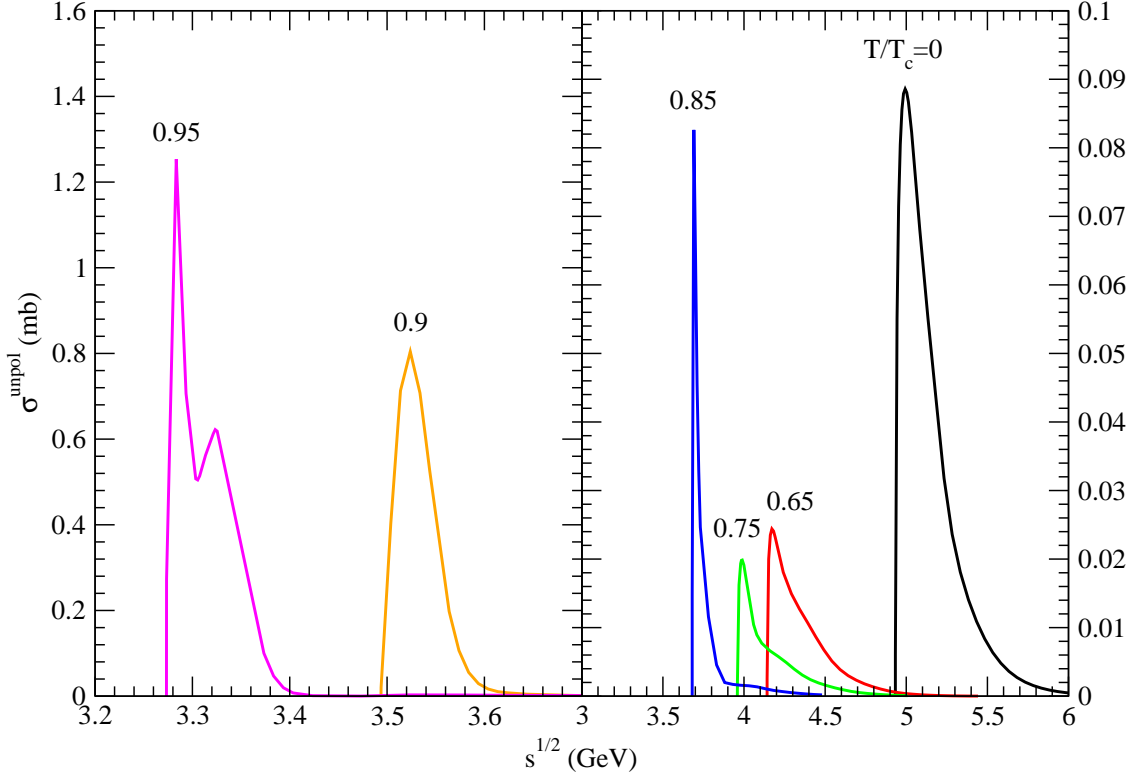


Figure 1: Cross sections for $D_s^+ \bar{D} \rightarrow K^* \psi(4040)$ at various temperatures.

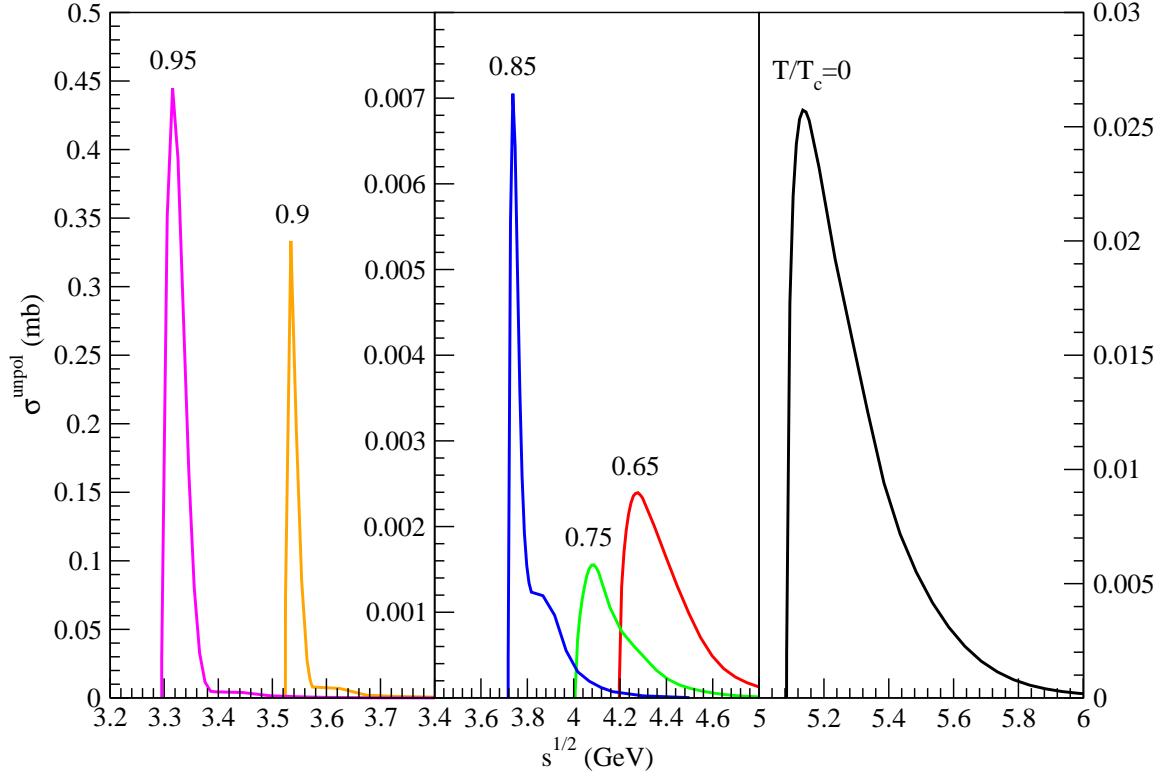


Figure 2: Cross sections for $D_s^+ \bar{D} \rightarrow K^* \psi(4160)$ at various temperatures.

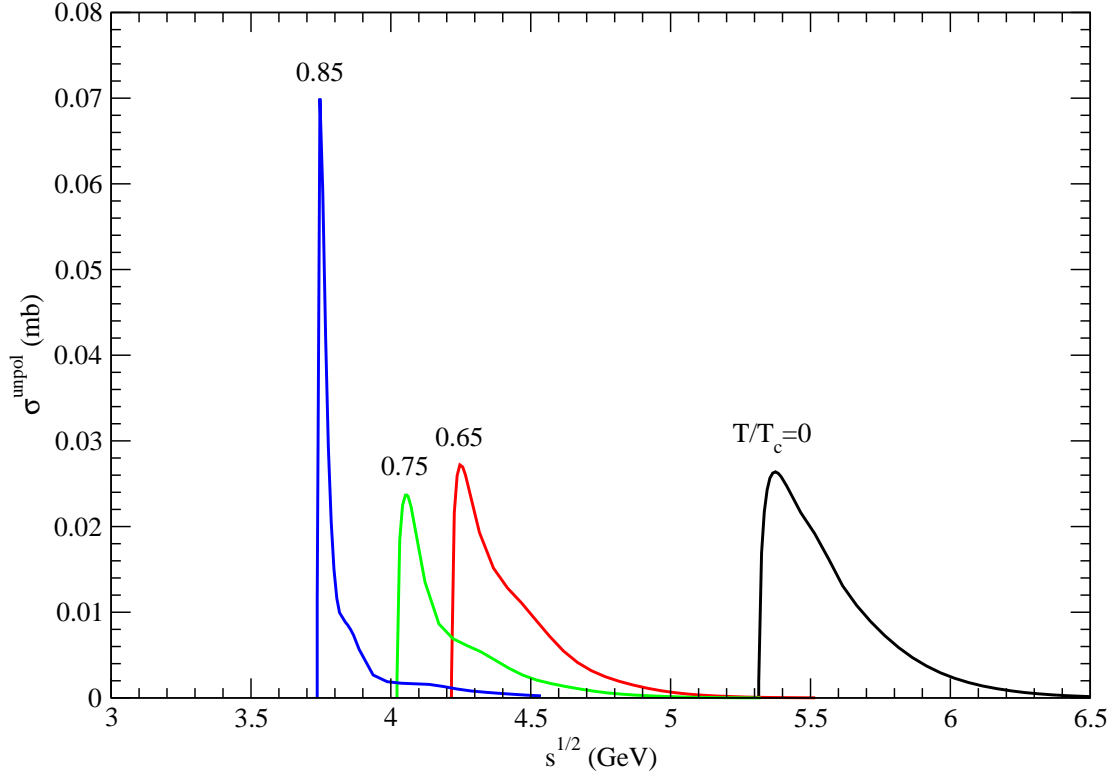


Figure 3: Cross sections for $D_s^+ \bar{D} \rightarrow K^* \psi(4415)$ at various temperatures.

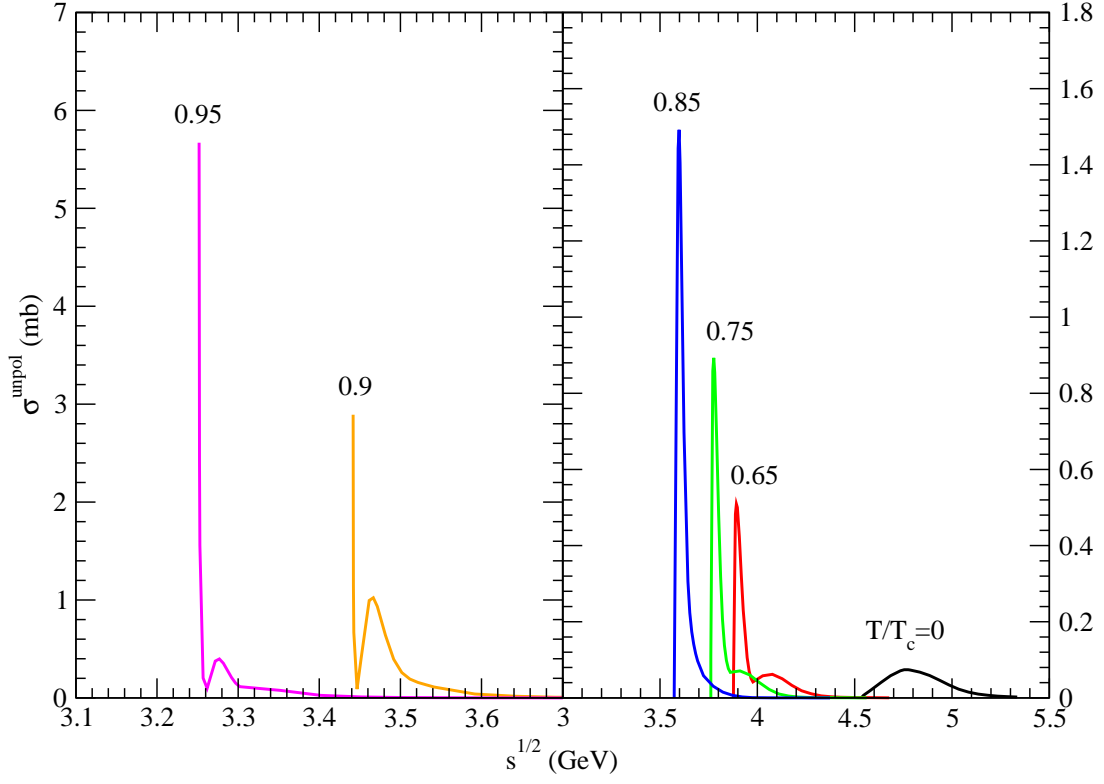


Figure 4: Cross sections for $D_s^+ \bar{D}^* \rightarrow K \psi(4040)$ at various temperatures.

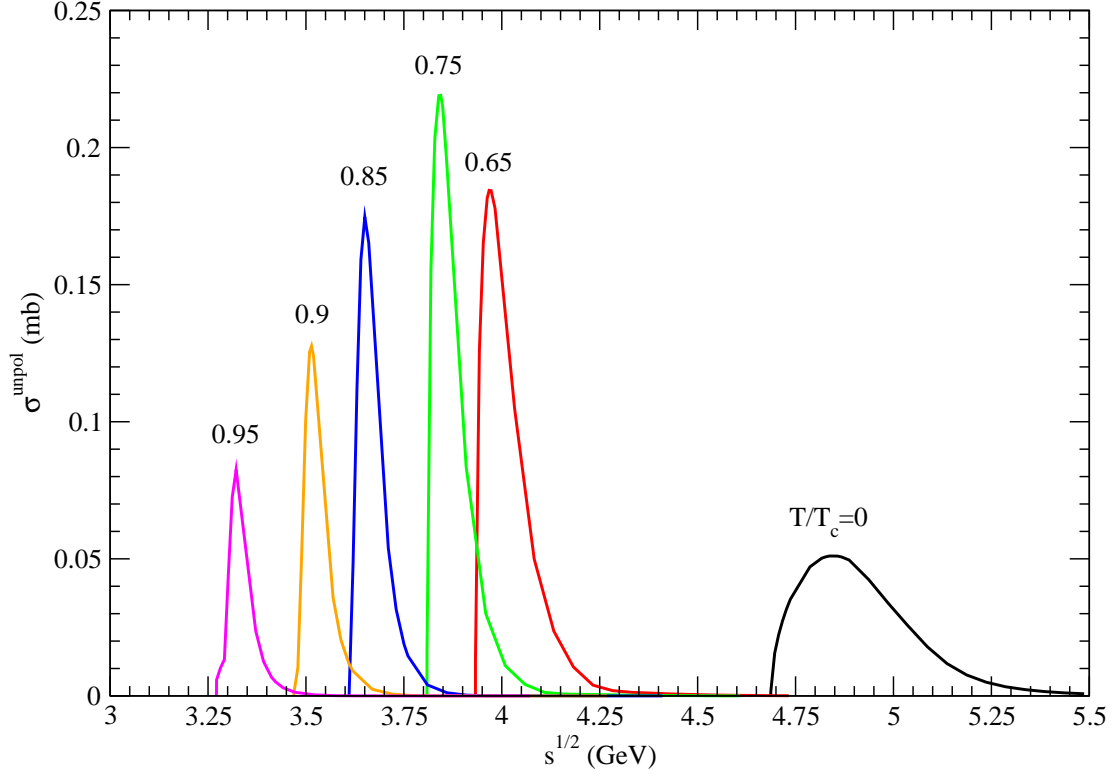


Figure 5: Cross sections for $D_s^+ \bar{D}^* \rightarrow K \psi(4160)$ at various temperatures.

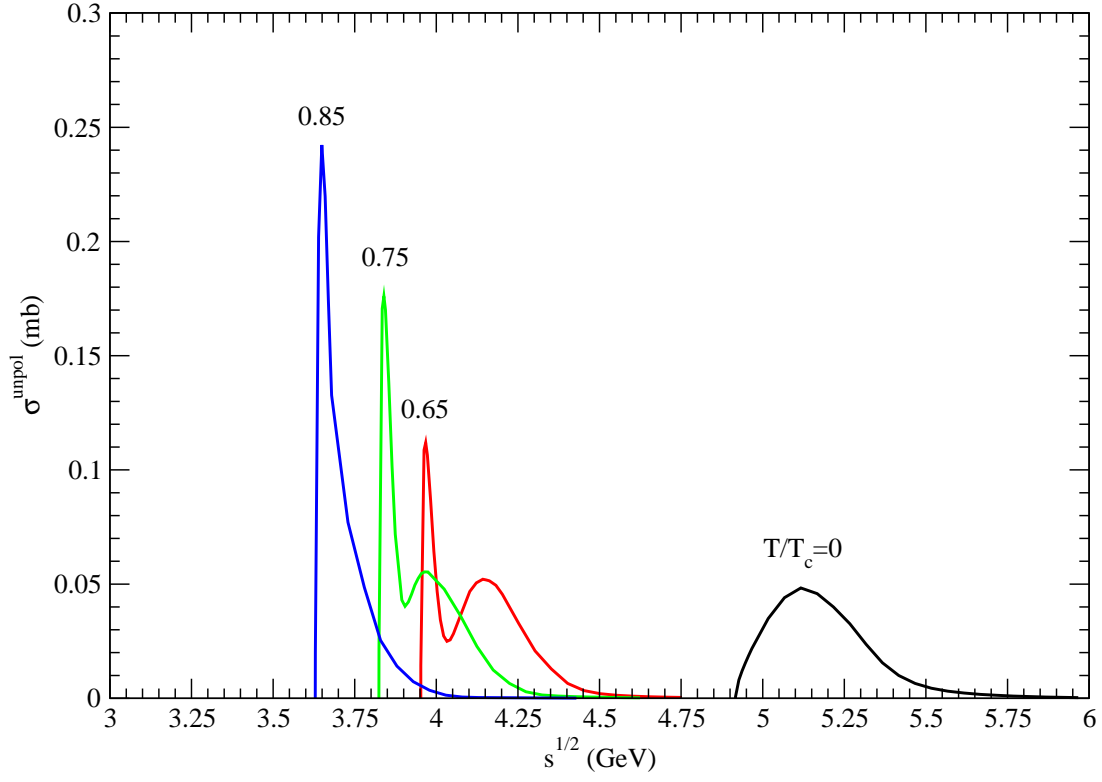


Figure 6: Cross sections for $D_s^+ \bar{D}_s^* \rightarrow K \psi(4415)$ at various temperatures.

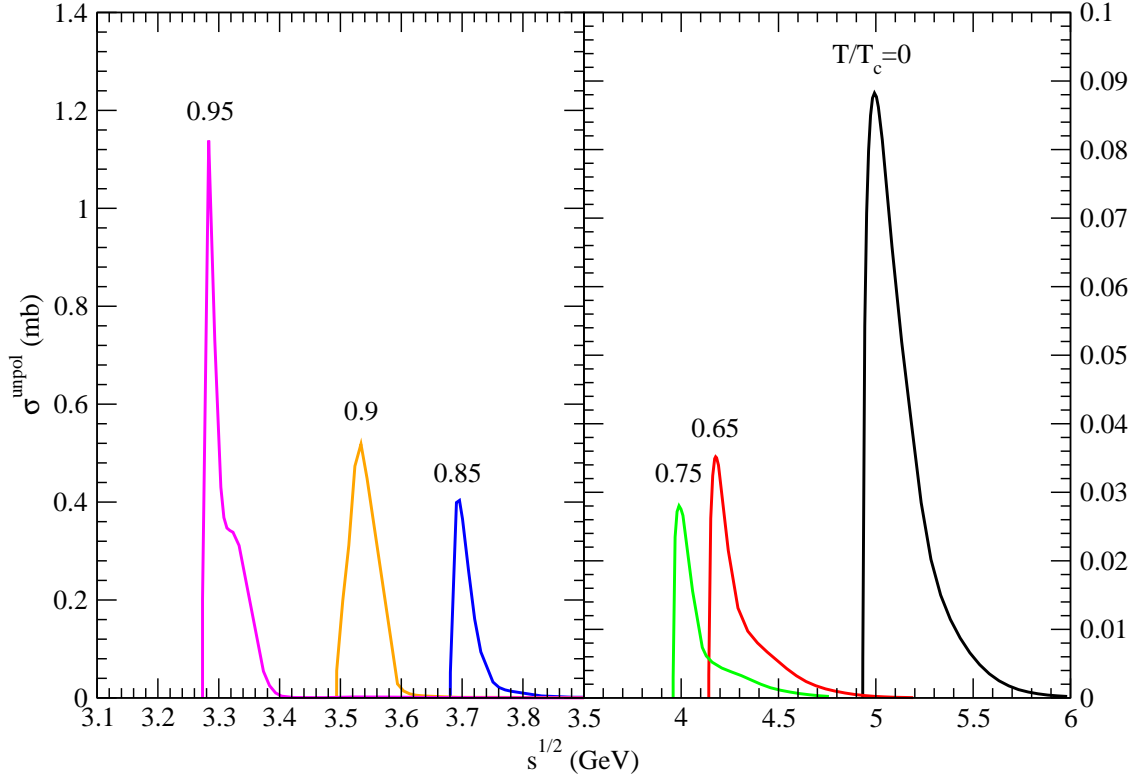


Figure 7: Cross sections for $D_s^+ \bar{D}_s^* \rightarrow K^* \psi(4040)$ at various temperatures.

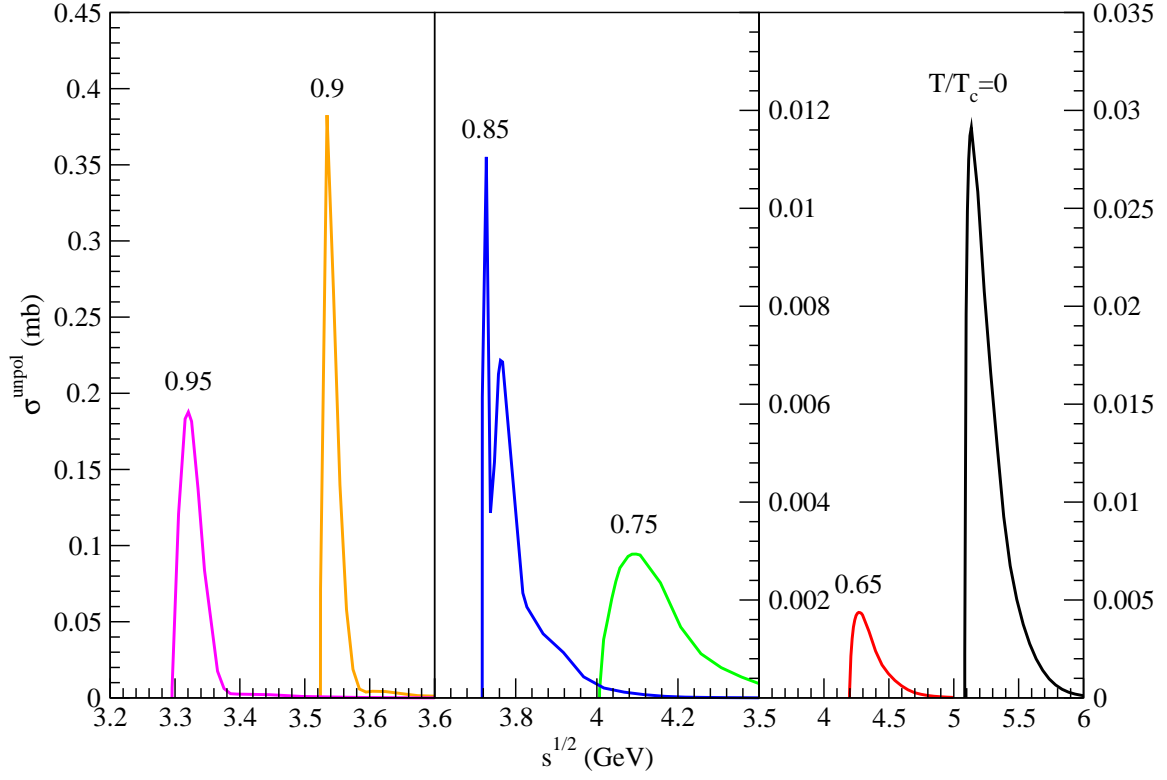


Figure 8: Cross sections for $D_s^+ \bar{D}_s^* \rightarrow K^* \psi(4160)$ at various temperatures.

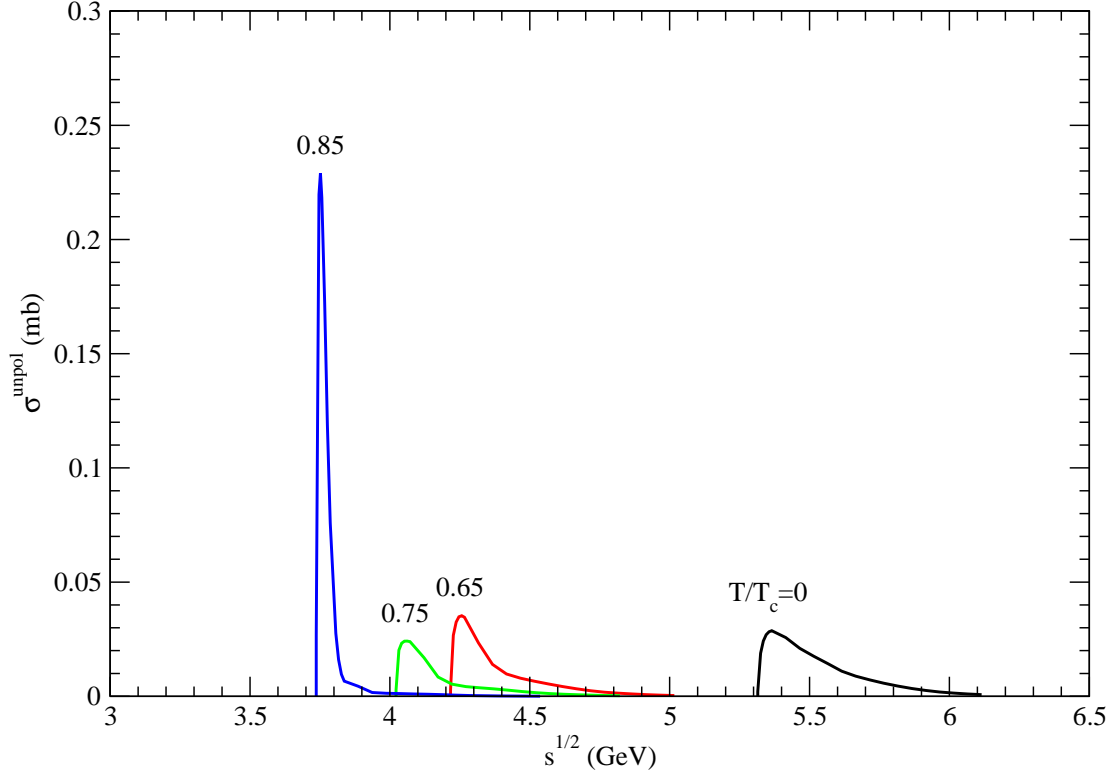


Figure 9: Cross sections for $D_s^+ \bar{D}^* \rightarrow K^* \psi(4415)$ at various temperatures.

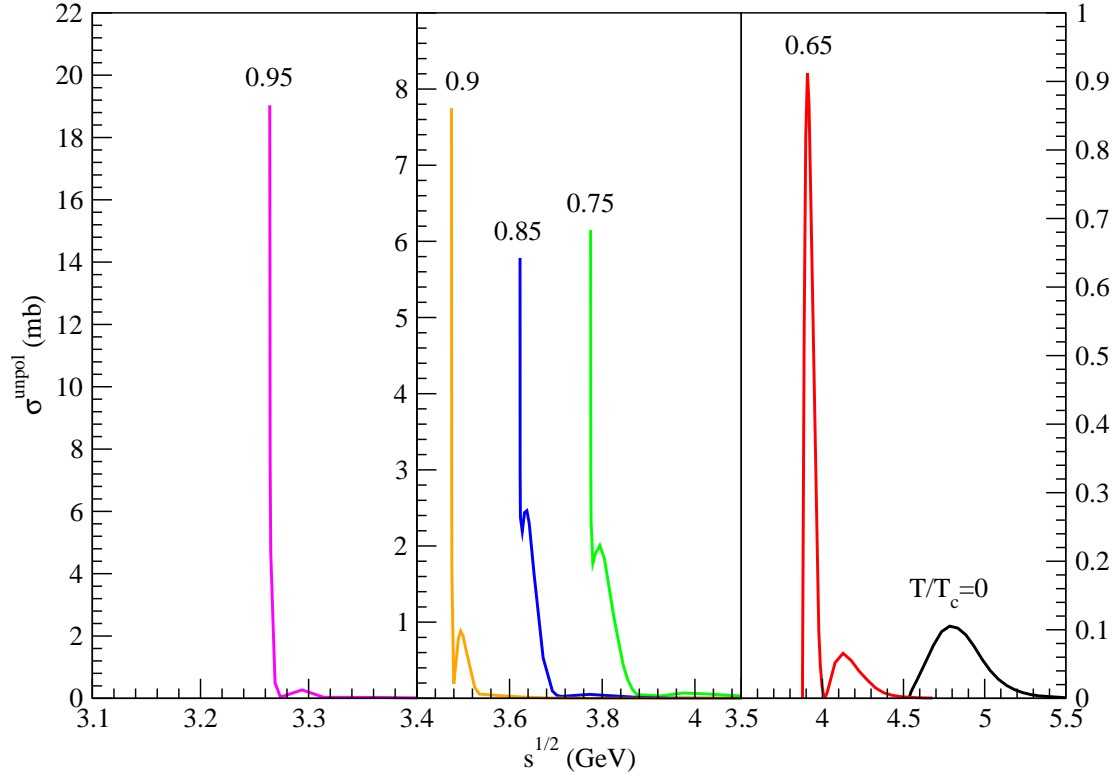


Figure 10: Cross sections for $D_s^{*+} \bar{D} \rightarrow K \psi(4040)$ at various temperatures.

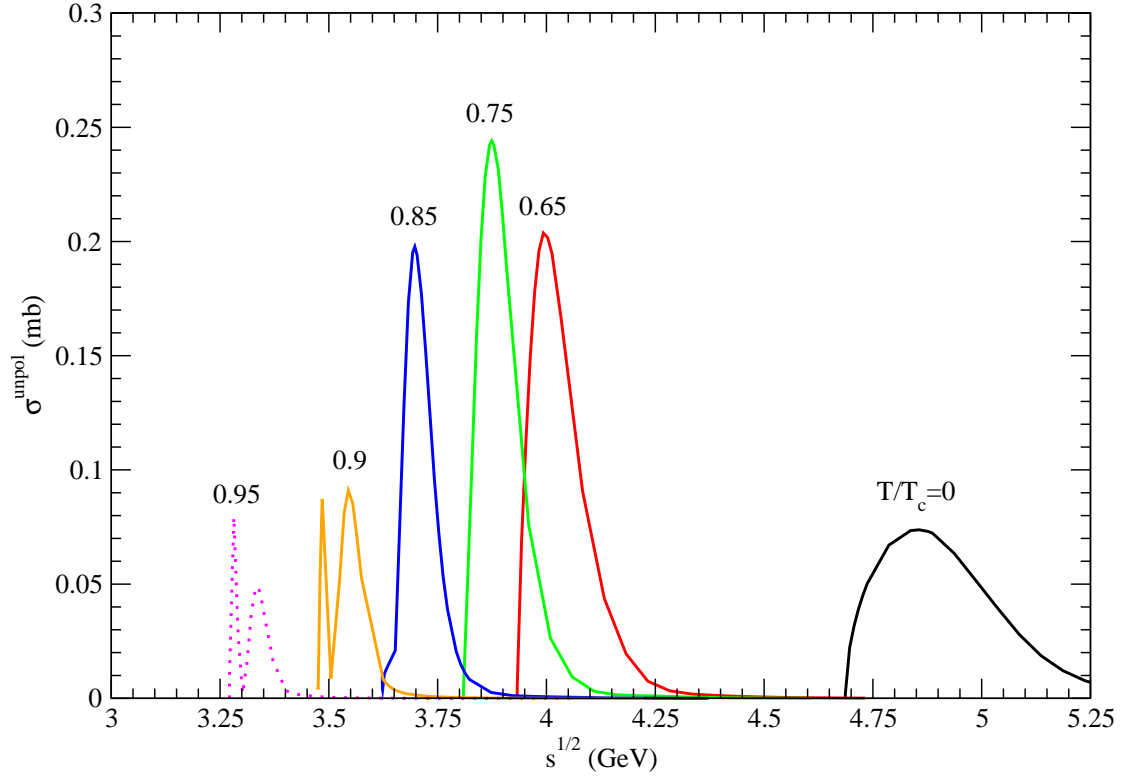


Figure 11: Cross sections for $D_s^{*+} \bar{D} \rightarrow K \psi(4160)$ at various temperatures.

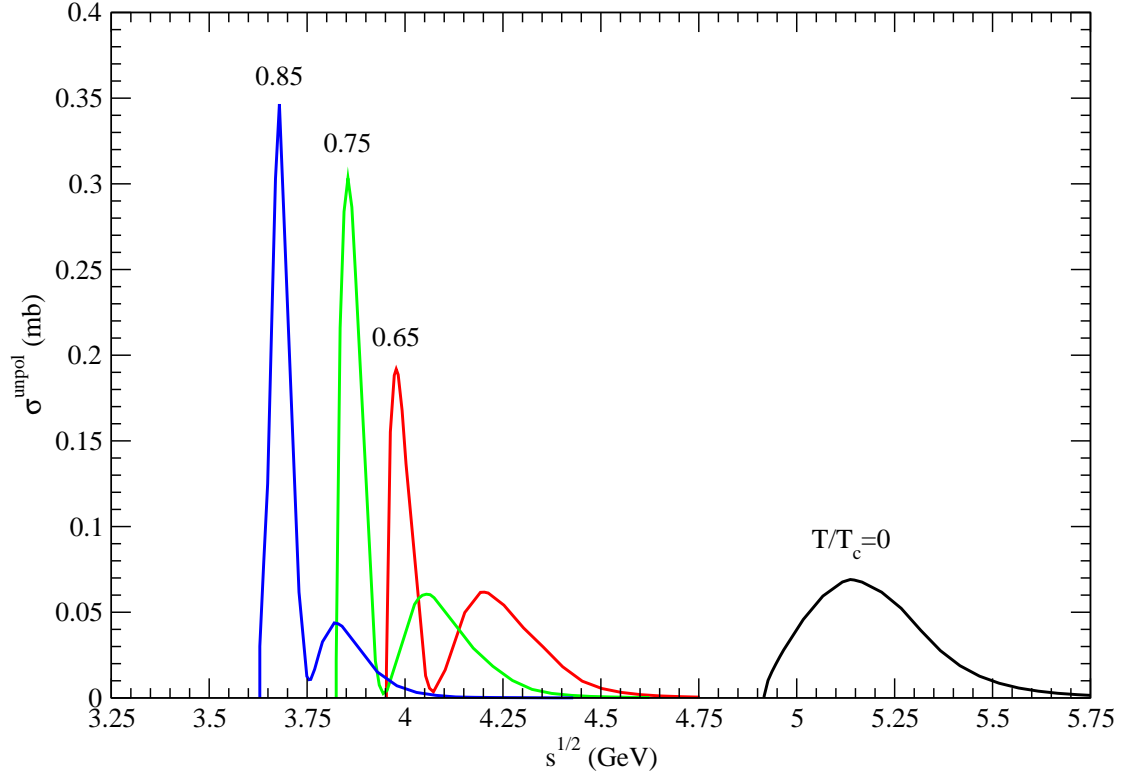


Figure 12: Cross sections for $D_s^{*+} \bar{D} \rightarrow K \psi(4415)$ at various temperatures.

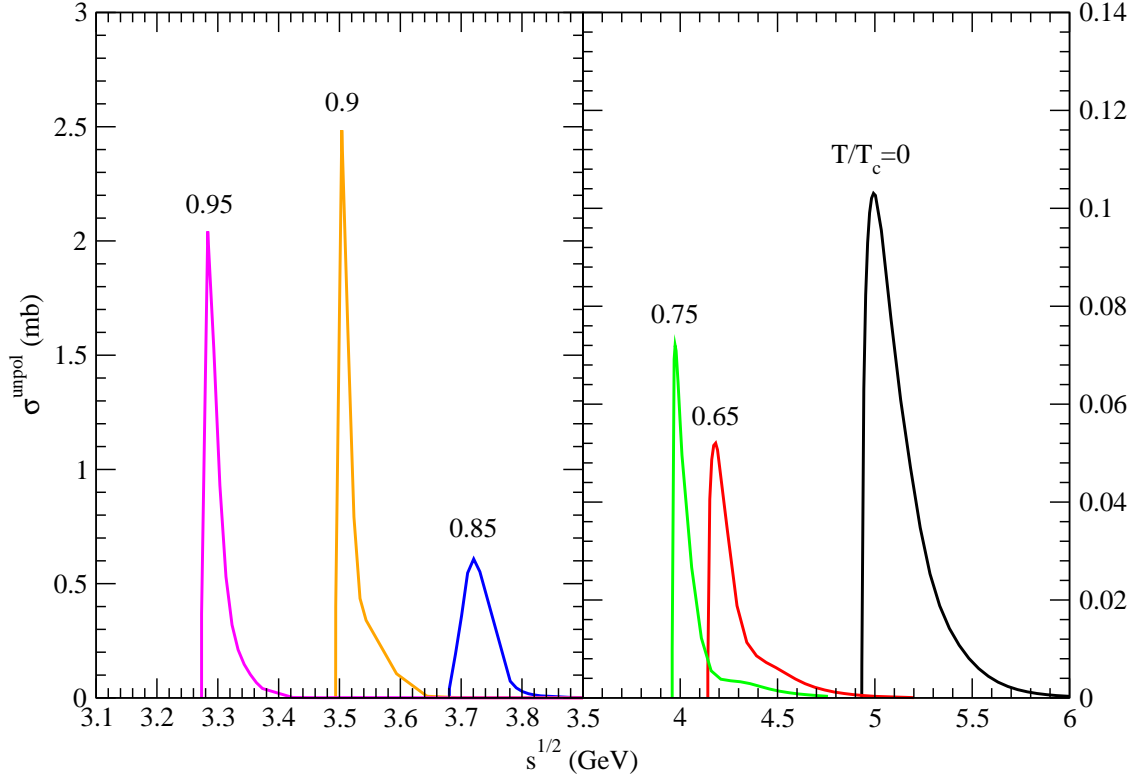


Figure 13: Cross sections for $D_s^{*+} \bar{D} \rightarrow K^* \psi(4040)$ at various temperatures.

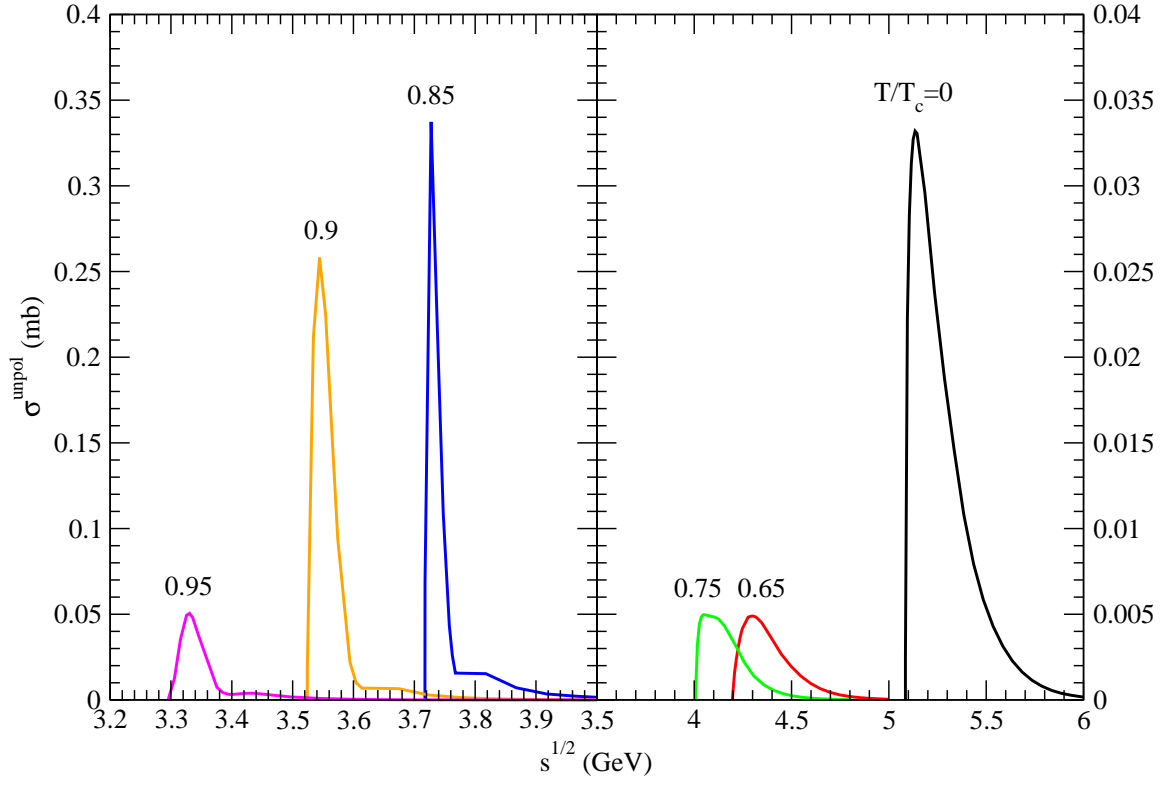


Figure 14: Cross sections for $D_s^{*+} \bar{D} \rightarrow K^* \psi(4160)$ at various temperatures.

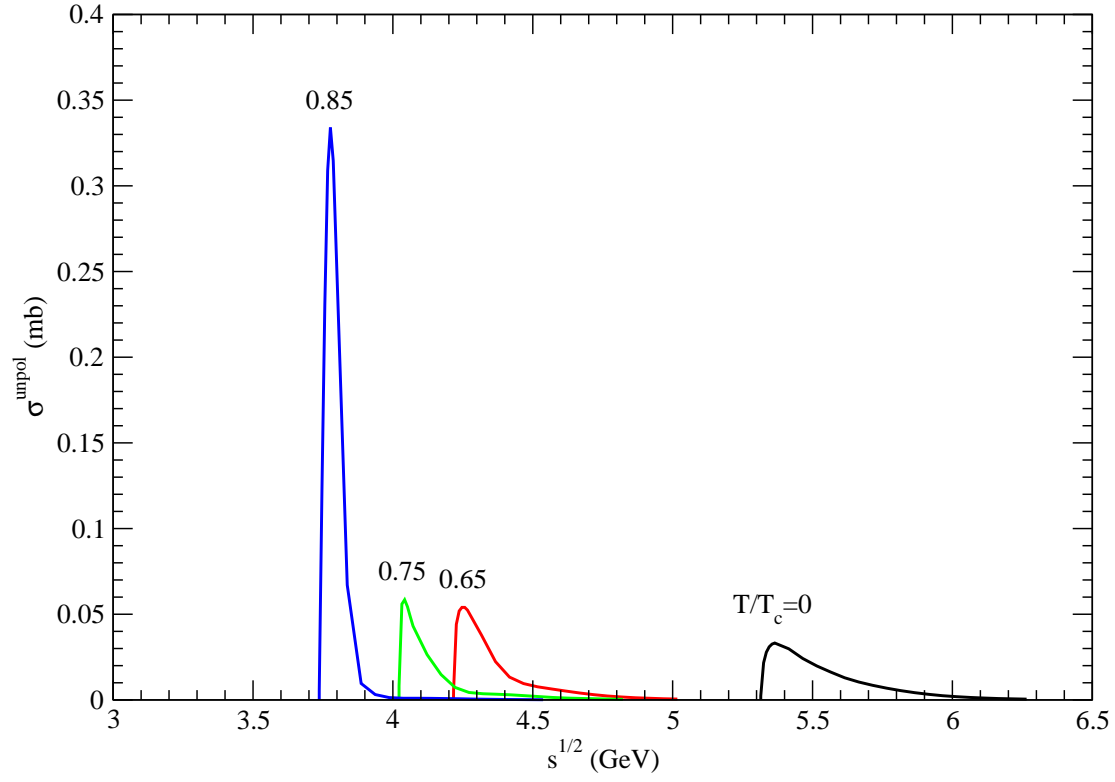


Figure 15: Cross sections for $D_s^{*+} \bar{D} \rightarrow K^* \psi(4415)$ at various temperatures.

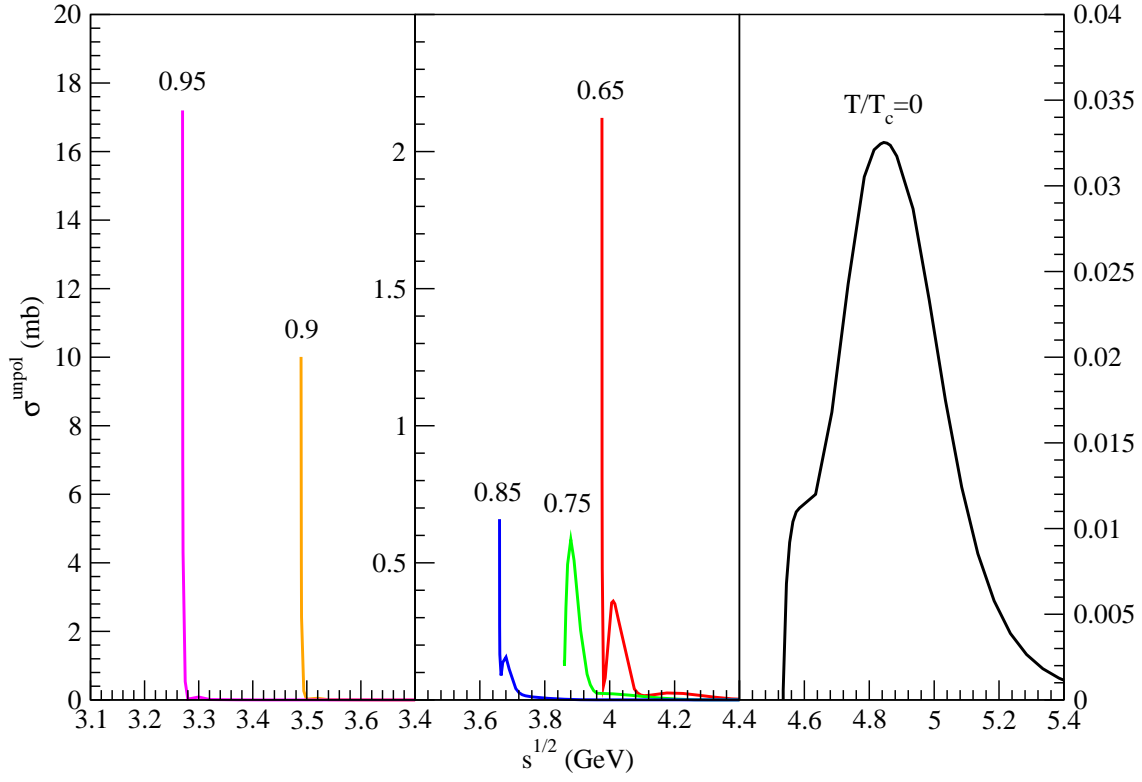


Figure 16: Cross sections for $D_s^{*+} \bar{D}^* \rightarrow K \psi(4040)$ at various temperatures.

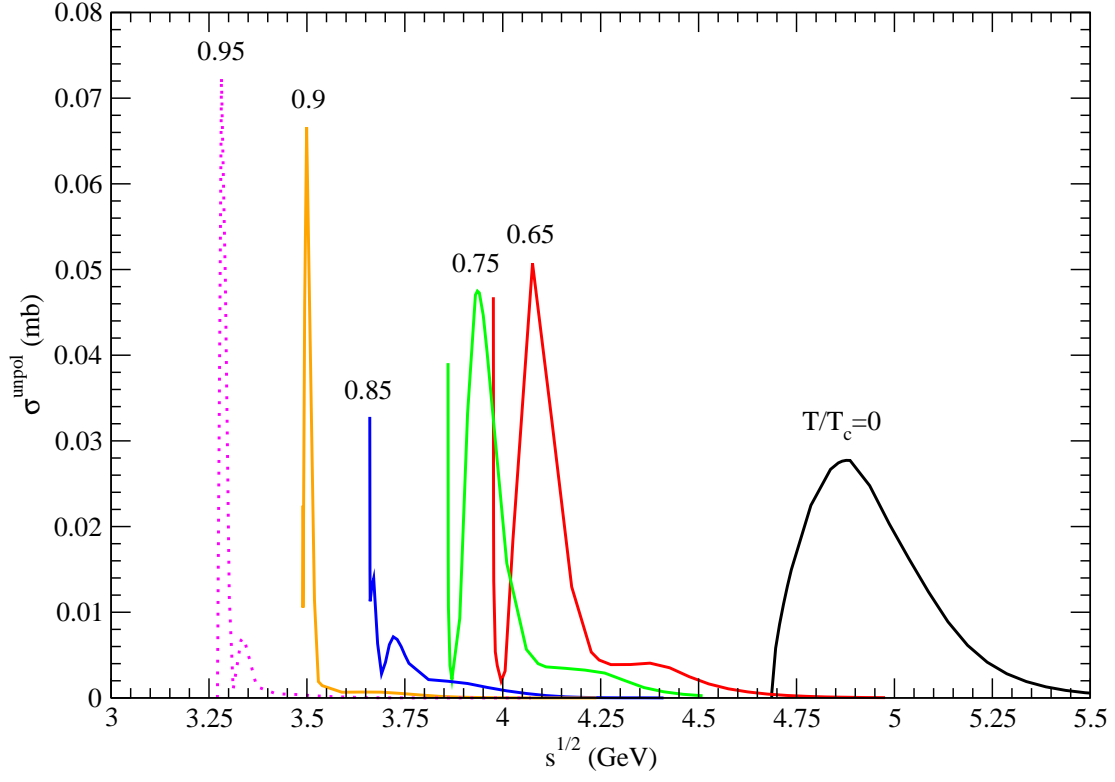


Figure 17: Cross sections for $D_s^{*+} \bar{D}^* \rightarrow K \psi(4160)$ at various temperatures.

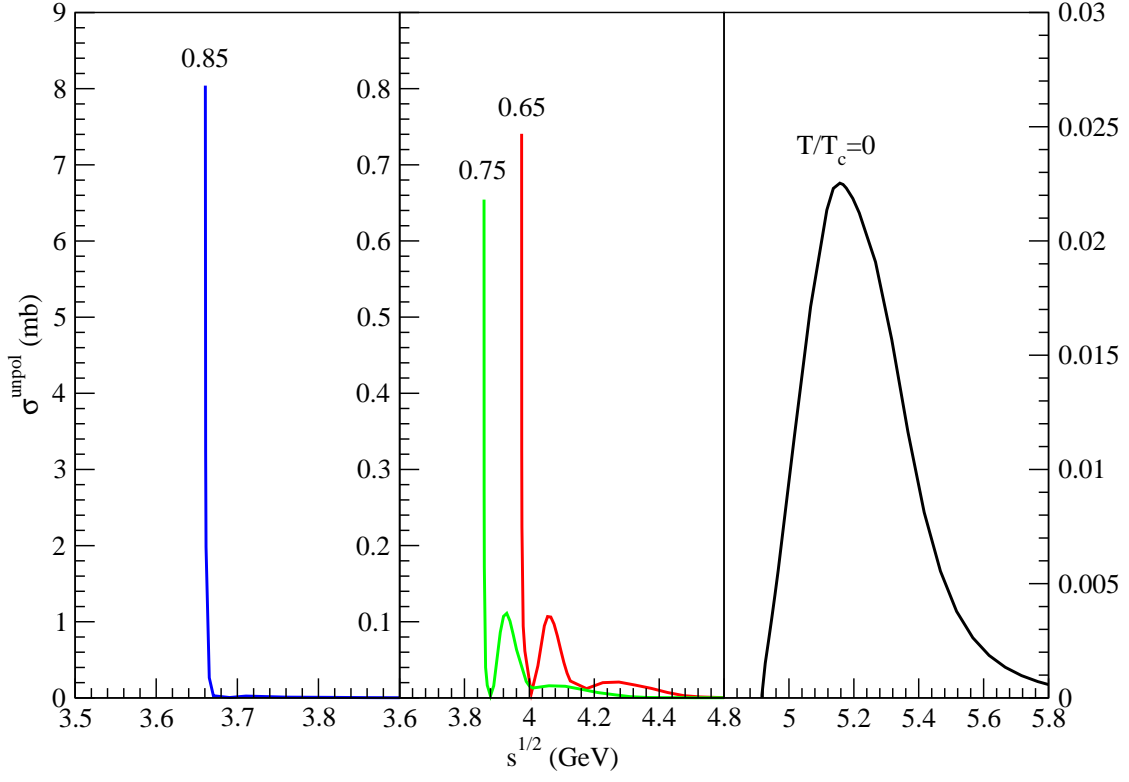


Figure 18: Cross sections for $D_s^{*+} \bar{D}^* \rightarrow K \psi(4415)$ at various temperatures.

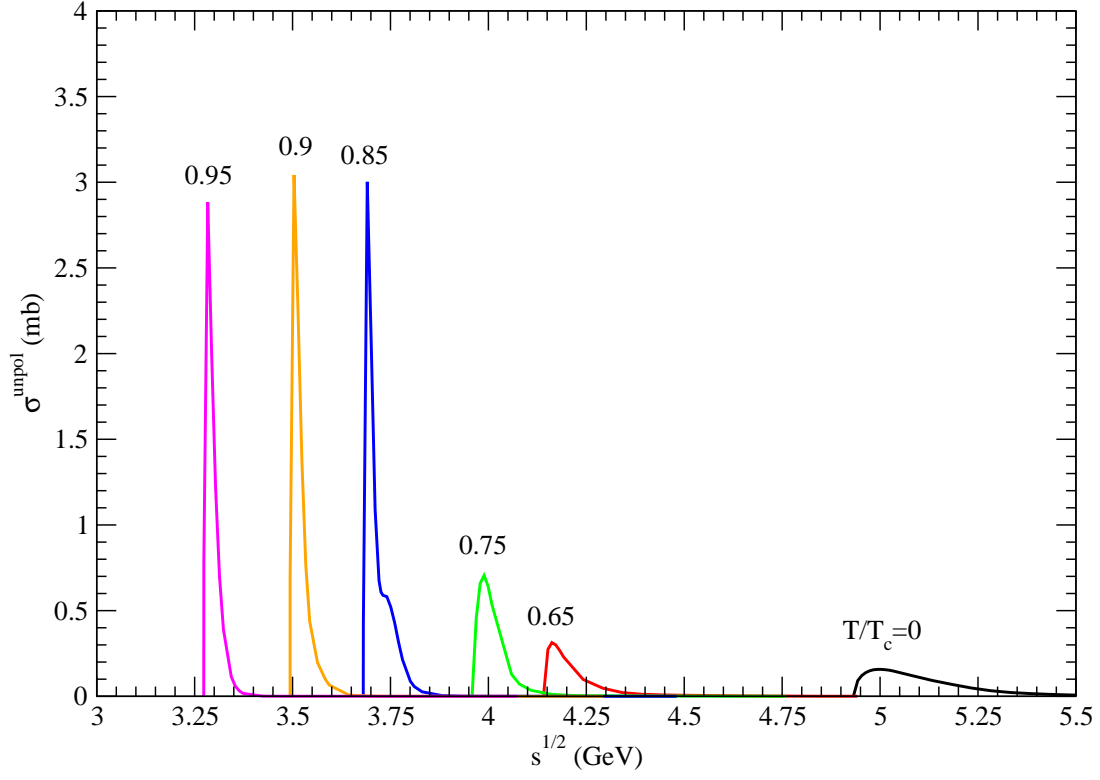


Figure 19: Cross sections for $D_s^{*+} \bar{D}^* \rightarrow K^* \psi(4040)$ at various temperatures.

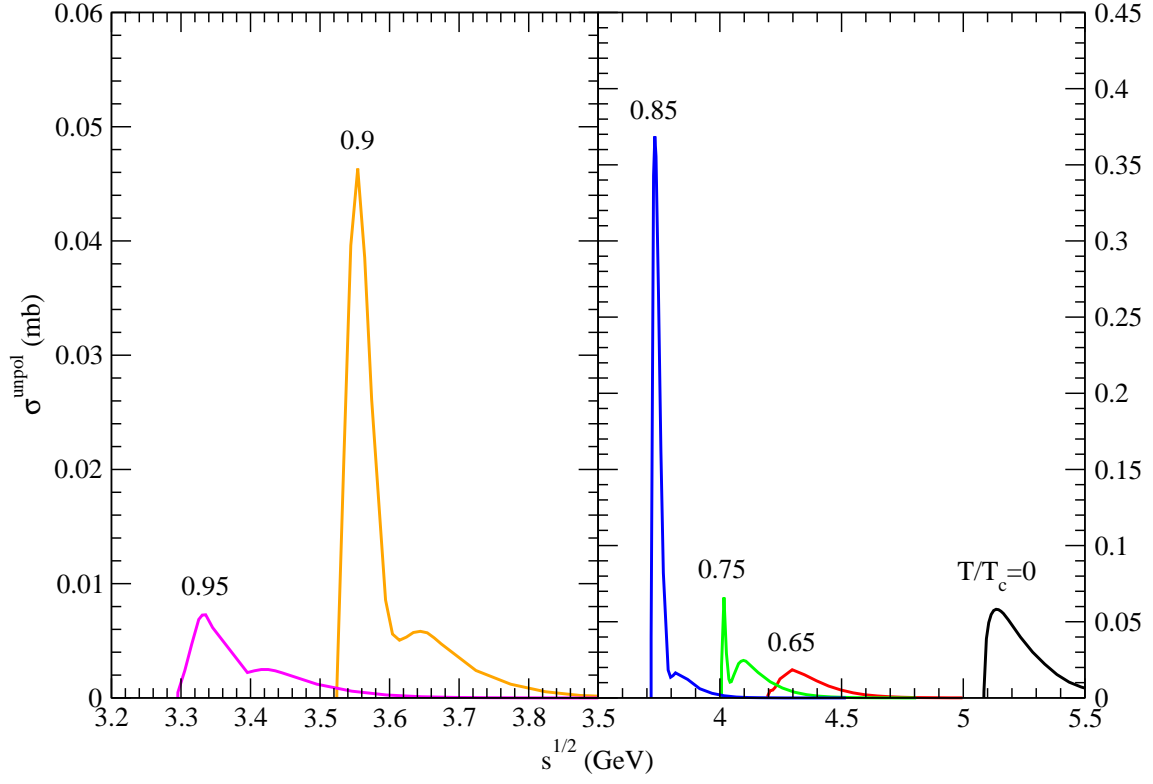


Figure 20: Cross sections for $D_s^{*+} \bar{D}^* \rightarrow K^* \psi(4160)$ at various temperatures.

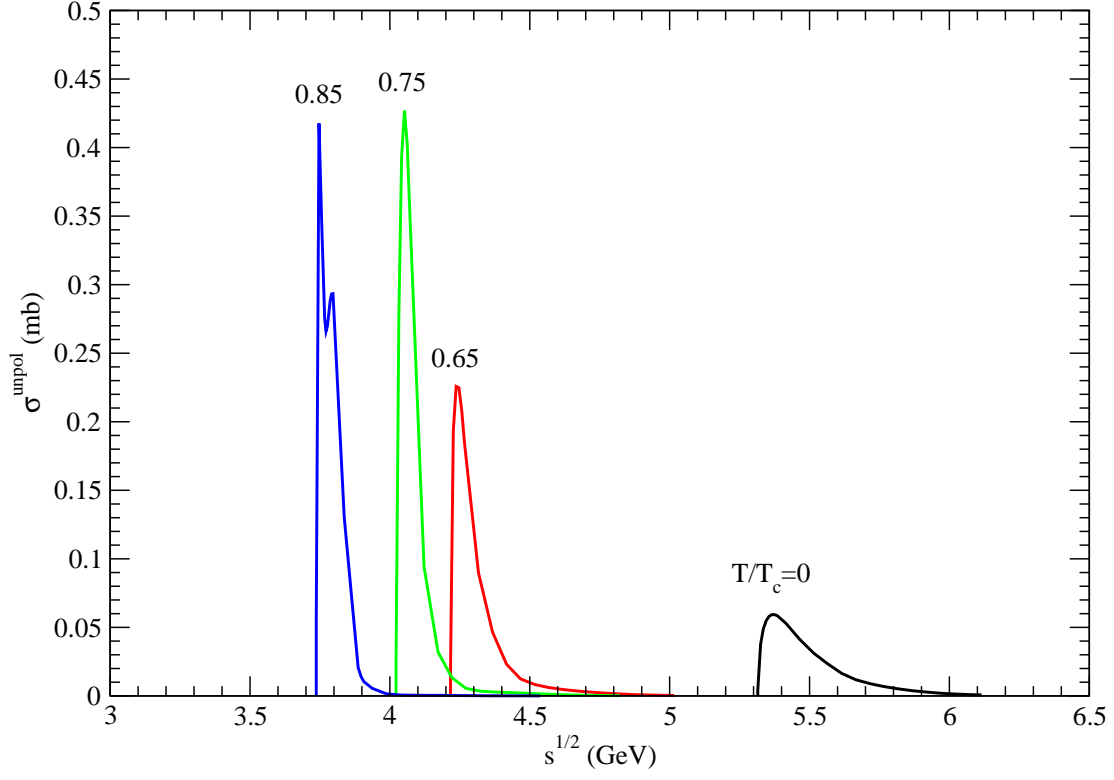


Figure 21: Cross sections for $D_s^{*+} \bar{D}^* \rightarrow K^* \psi(4415)$ at various temperatures.

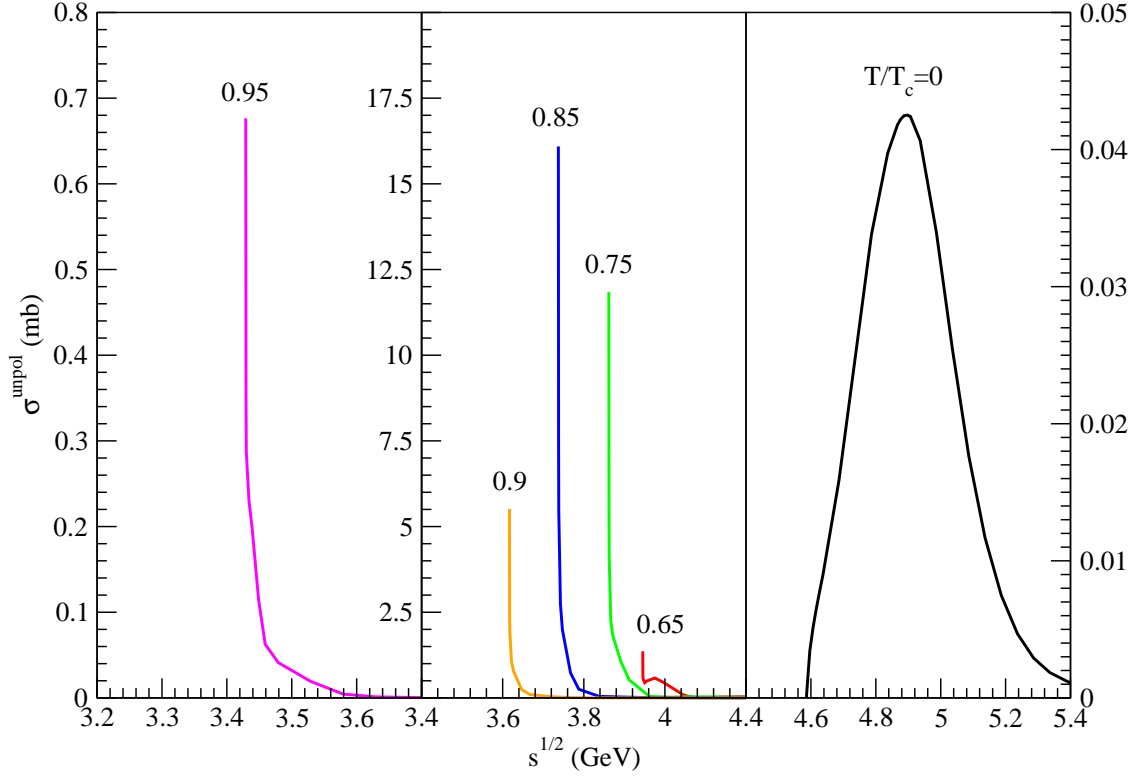


Figure 22: Cross sections for $D_s^+ D_s^{*-} \rightarrow \eta \psi(4040)$ at various temperatures.

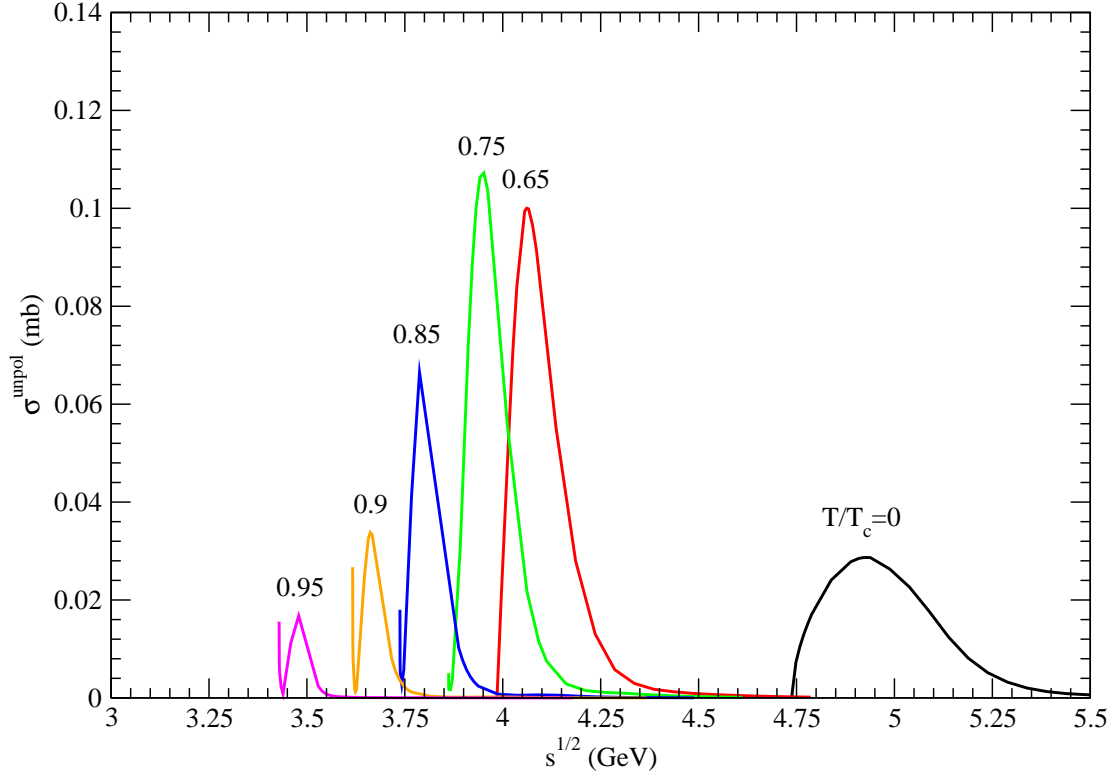


Figure 23: Cross sections for $D_s^+ D_s^{*-} \rightarrow \eta \psi(4160)$ at various temperatures.

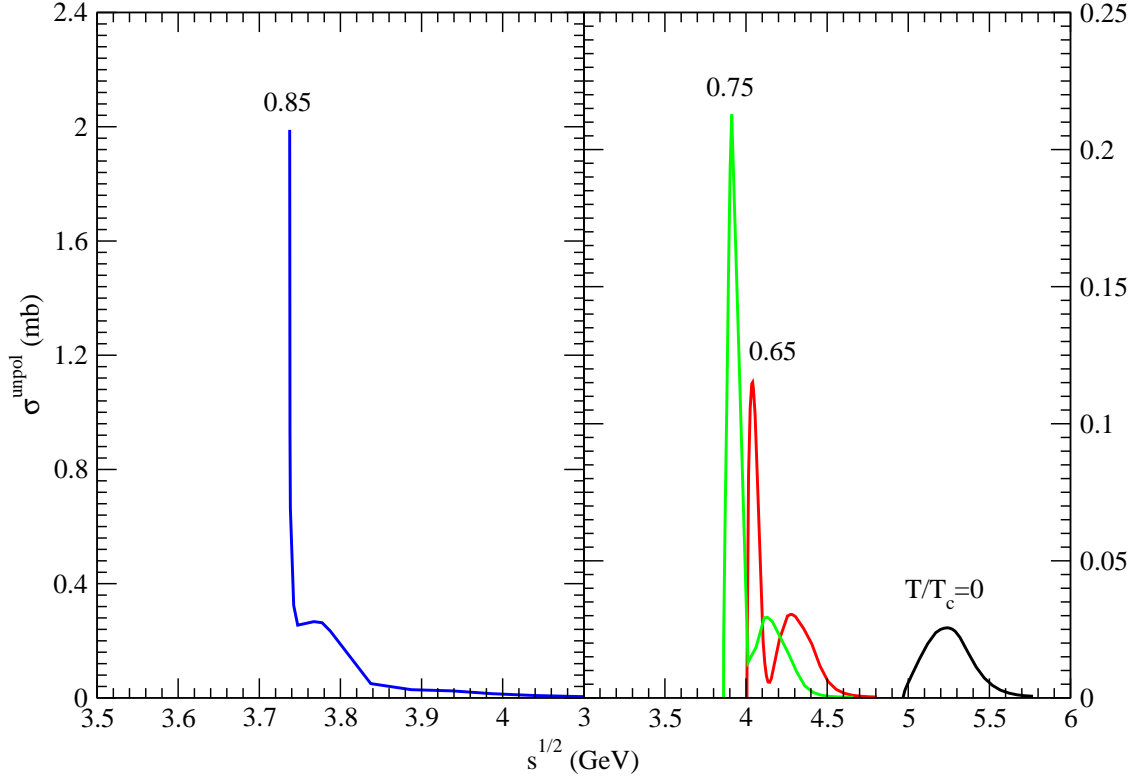


Figure 24: Cross sections for $D_s^+ D_s^{*-} \rightarrow \eta \psi(4415)$ at various temperatures.

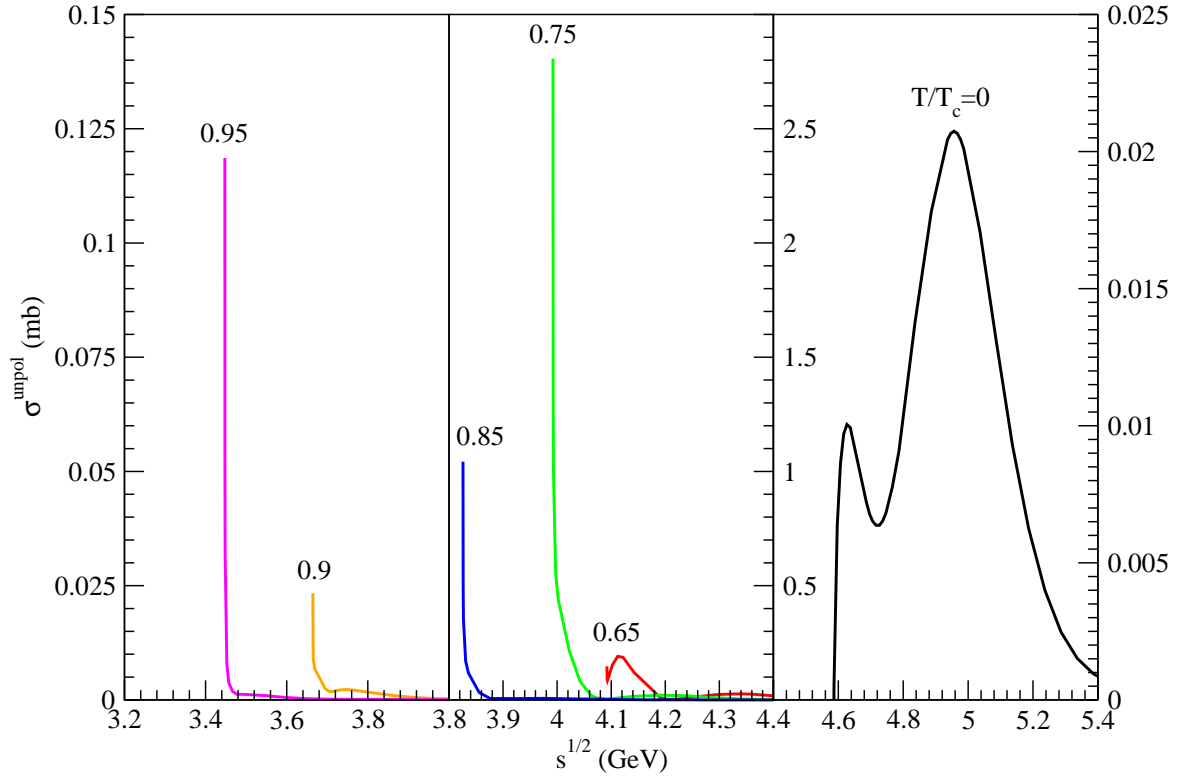


Figure 25: Cross sections for $D_s^{*+} D_s^{*-} \rightarrow \eta \psi(4040)$ at various temperatures.

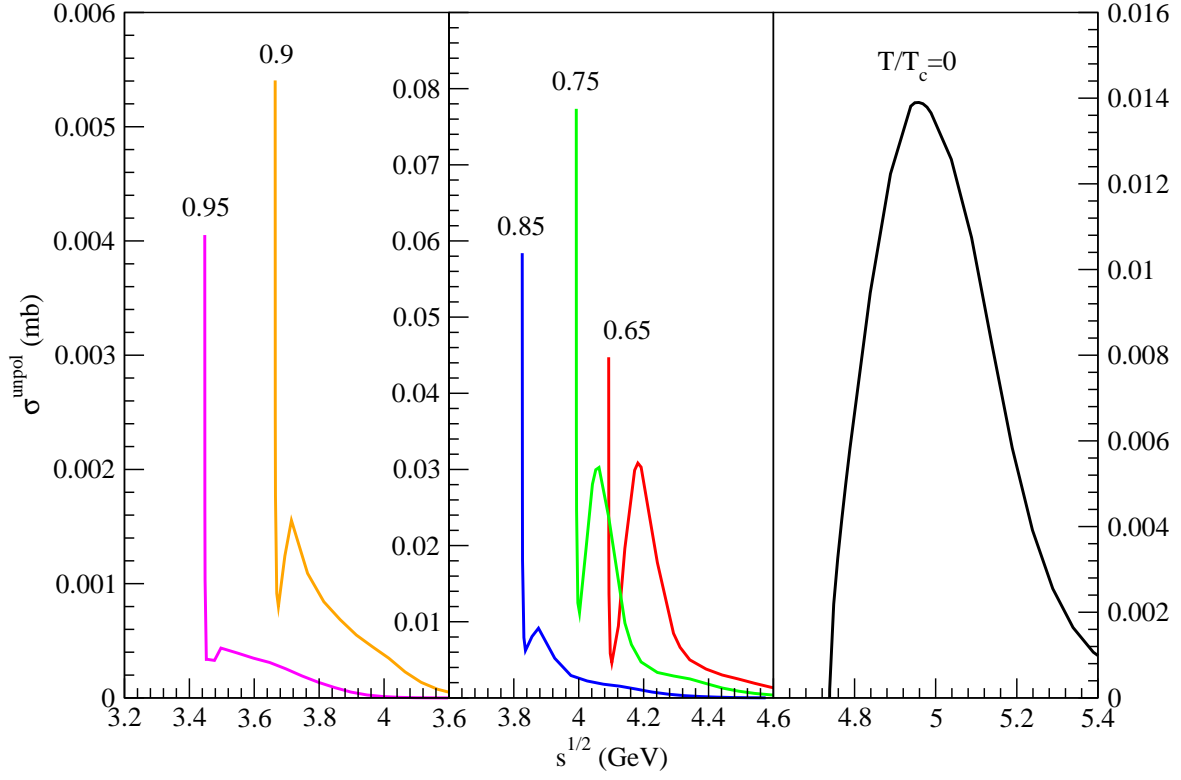


Figure 26: Cross sections for $D_s^{*+} D_s^{*-} \rightarrow \eta \psi(4160)$ at various temperatures.

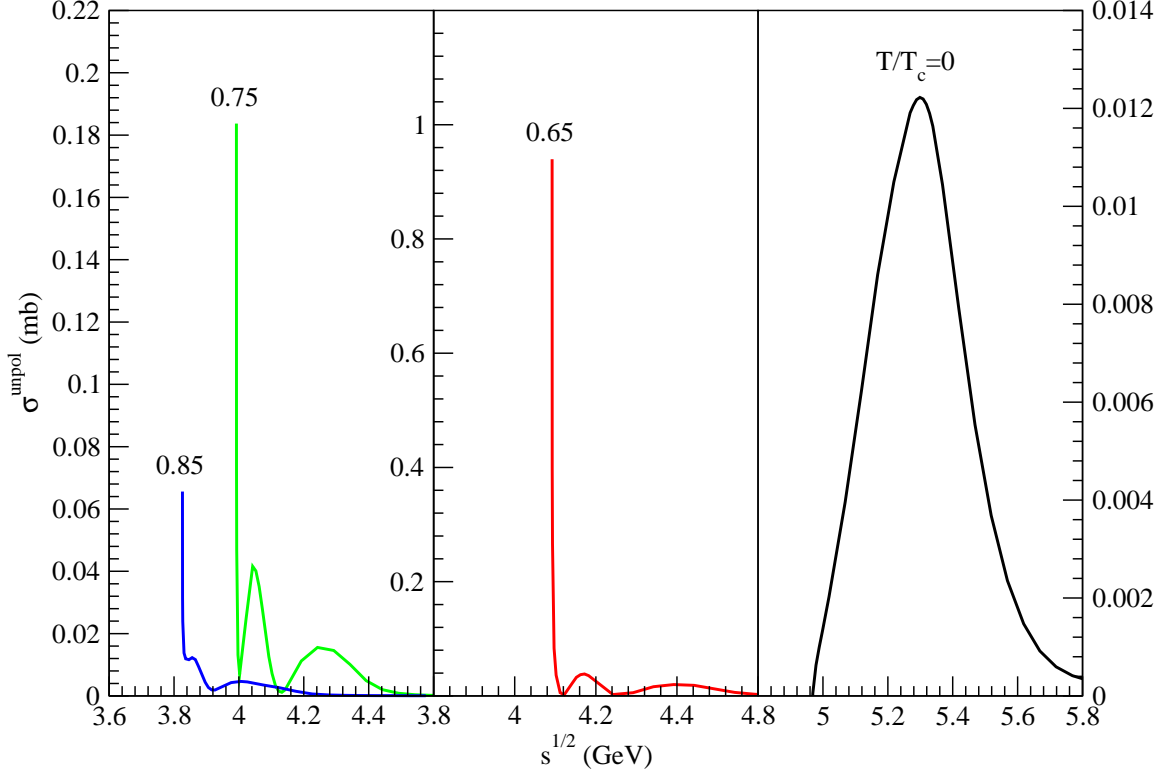


Figure 27: Cross sections for $D_s^{*+} D_s^{*-} \rightarrow \eta \psi(4415)$ at various temperatures.

Since the naive quark model was proposed by Gell-Mann and Zweig in 1964, cross sections for meson-meson scattering was first thought to be four times the cross section for quark-quark scattering. However, this additive picture of cross sections has been deemed to be approximate since QCD was established. One reason is that the cross section for elastic quark-quark scattering is not identical to the one for elastic quark-antiquark scattering which involves quark-antiquark annihilation and creation [48]. Assuming wave functions of both initial and final quarks and antiquarks are plane waves, the cross sections for quark-quark scattering and quark-antiquark scattering were obtained in perturbative QCD. In low-energy meson-meson scattering confinement of quarks and antiquarks in mesons needs to be taken into account. Wave functions of both initial and final quarks and antiquarks are no longer plane waves, and cross sections look like those in Figs. 1-27. In the present work low-energy meson-meson scattering produces two mesons. When the total center-of-mass energy increases, three, four, and more mesons are produced. Two-to-three meson-meson scattering, two-to-four meson-meson scattering, and so on lead to

finite cross sections for meson-meson scattering.

At zero temperature all reactions shown in Figs. 1-27 are endothermic. However, at $T = 0.65T_c, 0.75T_c, 0.85T_c, 0.9T_c,$ or $0.95T_c,$ a reaction may be endothermic or exothermic. Hence, we use the following two expressions to parametrize the numerical cross sections shown in Figs. 1-27:

$$\begin{aligned} \sigma^{\text{unpol}}(\sqrt{s}, T) = & a_1 \left(\frac{\sqrt{s} - \sqrt{s_0}}{b_1} \right)^{c_1} \exp \left[c_1 \left(1 - \frac{\sqrt{s} - \sqrt{s_0}}{b_1} \right) \right] \\ & + a_2 \left(\frac{\sqrt{s} - \sqrt{s_0}}{b_2} \right)^{c_2} \exp \left[c_2 \left(1 - \frac{\sqrt{s} - \sqrt{s_0}}{b_2} \right) \right], \end{aligned} \quad (11)$$

for endothermic reactions and

$$\begin{aligned} \sigma^{\text{unpol}}(\sqrt{s}, T) = & \frac{\vec{P}'^2}{\vec{P}^2} \left\{ a_1 \left(\frac{\sqrt{s} - \sqrt{s_0}}{b_1} \right)^{c_1} \exp \left[c_1 \left(1 - \frac{\sqrt{s} - \sqrt{s_0}}{b_1} \right) \right] \right. \\ & \left. + a_2 \left(\frac{\sqrt{s} - \sqrt{s_0}}{b_2} \right)^{c_2} \exp \left[c_2 \left(1 - \frac{\sqrt{s} - \sqrt{s_0}}{b_2} \right) \right] \right\}, \end{aligned} \quad (12)$$

for exothermic reactions. $\sqrt{s_0}$ is the threshold energy. In order to use the two parametrizations in the master rate equations, we need the separation (d_0) between the peak's location on the \sqrt{s} axis and the threshold energy and the square root ($\sqrt{s_z}$) of the Mandelstam variable at which the cross section is 1/100 of the peak cross section. Values of $a_1, b_1, c_1, a_2, b_2, c_2, d_0,$ and $\sqrt{s_z}$ are listed in Tables 1-9.

The expression on the right-hand side of Eq. (11) equals 0 at $\sqrt{s} = \sqrt{s_0}$, and thus can be used to parametrize numerical cross sections for endothermic reactions. Denote the spins of mesons $c\bar{q}_2, q_1\bar{c}, q_1\bar{q}_2,$ and $c\bar{c}$ by $S_{c\bar{q}_2}, S_{q_1\bar{c}}, S_{q_1\bar{q}_2},$ and $S_{c\bar{c}},$ respectively. If the reaction $c\bar{q}_2 + q_1\bar{c} \rightarrow q_1\bar{q}_2 + c\bar{c}$ is exothermic, its cross section can be related to the endothermic reaction $q_1\bar{q}_2 + c\bar{c} \rightarrow c\bar{q}_2 + q_1\bar{c}$ by the detailed balance

$$\sigma_{c\bar{q}_2+q_1\bar{c} \rightarrow q_1\bar{q}_2+c\bar{c}}^{\text{unpol}} = \frac{(2S_{q_1\bar{q}_2} + 1)(2S_{c\bar{c}} + 1)}{(2S_{c\bar{q}_2} + 1)(2S_{q_1\bar{c}} + 1)} \frac{\vec{P}'^2}{\vec{P}^2} \sigma_{q_1\bar{q}_2+c\bar{c} \rightarrow c\bar{q}_2+q_1\bar{c}}^{\text{unpol}} \quad (13)$$

Hence, the expression on the right-hand side of Eq. (12) has the factor $\vec{P}'^2/\vec{P}^2.$

We study the production of $\psi(4040), \psi(4160),$ and $\psi(4415)$ mesons in central Pb-Pb collisions at the LHC. Hadronic matter possesses cylindrical symmetry, and the hydrodynamic equation is solved in terms of the cylindrical polar coordinates (r, ϕ, z) [20],

where the z -axis in the rest frame of hadronic matter is set along the moving direction of a nucleus and passes through the nuclear center, r is the distance from the fluid-element center to the z -axis, and ϕ is the azimuth. With the shear viscosity given in Ref. [22], the hydrodynamic equation provides the temperature and the transverse velocity of hadronic matter that expands.

In the source terms of the master rate equations $n_D, n_{\bar{D}}, n_{D^*}, n_{\bar{D}^*}, n_{D_s^+}, n_{D_s^-}, n_{D_s^{*+}},$ and $n_{D_s^{*-}}$ are obtained from momentum distribution functions of charmed mesons and charmed strange mesons. Unlike pion-pion scattering, cross sections for pion scattering by open-charm mesons are small. Thermal states of open-charm mesons may not be established by such small cross sections. We give a Lorentz-invariant form of the momentum distribution functions of open-charm mesons,

$$f_i(k_i) = \frac{1 + \sum_{l=1}^{\infty} c_l (k_i \cdot u)^l}{e^{k_i \cdot u / T_{\text{dec}}} - 1}, \quad (14)$$

where T_{dec} is the inverse slope parameter. If $\sum_{l=1}^{\infty} c_l (k_i \cdot u)^l = 0$, $f_i(k_i)$ becomes the Bose-Einstein distribution function. The term $\sum_{l=1}^{\infty} c_l (k_i \cdot u)^l$ indicates deviation from thermal equilibrium. After fits to the experimental data [50] of dN/dp_T of prompt $D^+, D^0, D^{*+},$ and D_s^+ mesons at $p_T < 8$ GeV/ c in central Pb-Pb collisions at $\sqrt{s_{NN}} = 5.02$ TeV, values of l and c_l for $D^+, D^0,$ and D^{*+} mesons are listed in Ref. [19], and for D_s^+ mesons here,

$$l = 15, \quad c_l = 6 \times 10^{-17};$$

$$l \neq 15, \quad c_l = 0.$$

T_{dec} determined from the experimental data is 0.1686 GeV, and the value is close to the critical temperature. This means that open-charm mesons decouple early from hadronic matter. We thus use the momentum distribution functions (Eq. (14)) to obtain the average cross section defined in Eq. (3). Temperature dependence of the average cross section weighted by the relative velocity arises from temperature dependence of $\sigma_{ij \rightarrow i'j'}$ and of v_{ij} .

In central Pb-Pb collisions at $\sqrt{s_{NN}}=5.02$ TeV hadronic matter is produced at the proper time 10.05 fm/ c [19]. We start solving the hydrodynamic equation and the master

rate equations at the time, and get number densities at kinetic freeze-out. Using the momentum distribution functions $1/(e^{k_i \cdot u/T} - 1)$ for pions, kaons, and vector kaons in the Cooper-Frye formula [51], fits to the experimental data of momentum spectra [52, 53] to obtain the freeze-out time 21.07 fm/ c and the freeze-out temperature 0.126 GeV. The average cross sections in the last twenty-four terms on the right-hand side of Eq. (2) involve momentum distribution functions of $\psi(4040)$, $\psi(4160)$, and $\psi(4415)$. At present, we assume the distribution functions to take the form $\lambda_i/(e^{k_i \cdot u/T_i} - 1)$, where λ_i are constants and the inverse slope parameters T_i equal the dissociation temperatures of $\psi(4040)$, $\psi(4160)$, and $\psi(4415)$. We need not know values of λ_i , because λ_i in the numerator and in the denominator in Eq. (3) cancel each other out. Variation of number densities with respect to the proper time (τ) at $r = 0$ fm is drawn as upper solid, upper dashed, and upper dotted curves in Fig. 28, and r dependence at kinetic freeze-out is plotted as upper solid, upper dashed, and upper dotted curves in Fig. 29. Number densities of $\psi(4040)$, $\psi(4160)$, and $\psi(4415)$ mesons were obtained with an early version of FORTRAN code which numerically solves the master rate equations in Ref. [19]. After several errors are removed, a new version is used to calculate number densities, which are smaller than those shown in Ref. [19]. When the proper time increases from 10.83 fm/ c , 11.38 fm/ c , and 13.95 fm/ c , respectively, the number densities of $\psi(4040)$, $\psi(4160)$, and $\psi(4415)$ increase. However, the three mesons produced at $r = 0$ fm spread out, and this reduces the number densities. When the reduced amount exceeds the increased amount, the number densities decrease as seen in Fig. 28.

The upper solid, upper dashed, and upper dotted curves shown in Figs. 28 and 29 result from reactions between two charmed mesons, between a charmed meson and a charmed strange meson, and between two charmed strange mesons as well as their reverse reactions. To show contributions of charmed strange mesons in producing $\psi(4040)$, $\psi(4160)$, and $\psi(4415)$ mesons, we plot lower solid, lower dashed, and lower dotted curves that only result from reactions between two charmed mesons. From the lower curves to the upper curves changes of number densities are obvious. For example, the $\psi(4040)$, $\psi(4160)$, and $\psi(4415)$ number densities at kinetic freeze-out and at $r = 0$ increase by

19.2%, 14.5%, and 18.4%, respectively, due to the reactions of charmed strange mesons.

Table 1: Values of the parameters in Eq. (11) for $D_s^+ \bar{D} \rightarrow K^* \psi(4040)$, $K^* \psi(4160)$, and $K^* \psi(4415)$. a_1 and a_2 are in units of millibarns; b_1 , b_2 , d_0 , and $\sqrt{s_z}$ are in units of GeV; c_1 and c_2 are dimensionless.

final state	T/T_c	a_1	b_1	c_1	a_2	b_2	c_2	d_0	$\sqrt{s_z}$
$K^* \psi(4040)$	0	0.01	0.03	0.42	0.08	0.07	0.51	0.06	5.88
	0.65	0.011	0.183	1.91	0.023	0.0243	0.49	0.03	5.06
	0.75	0.008	0.07	0.26	0.013	0.024	0.9	0.03	4.87
	0.85	0.014	0.048	0.25	0.072	0.008	0.56	0.01	4.19
	0.9	0.21	0.007	0.71	0.76	0.031	3	0.03	3.62
	0.95	0.81	0.012	10.7	0.88	3.37	0.132	0.01	3.4
$K^* \psi(4160)$	0	0.004	0.02	0.55	0.023	0.07	0.48	0.05	5.95
	0.65	0.001	0.019	0.44	0.002	0.113	1.08	0.08	5.02
	0.75	0.0001	0.0003	1.22	0.00142	0.0727	0.7	0.08	4.77
	0.85	0.0016	0.024	0.29	0.0056	0.02	1.66	0.02	4.17
	0.9	0.08	0.0003	0.43	0.34	0.0086	1.11	0.01	3.66
	0.95	0.07	0.003	0.35	0.44	0.021	1.86	0.02	3.4
$K^* \psi(4415)$	0	0.005	0.025	0.59	0.023	0.088	0.47	0.06	6.41
	0.65	0.018	0.068	0.37	0.011	0.022	0.91	0.03	5.14
	0.75	0.006	0.123	0.19	0.019	0.03	0.8	0.035	4.93
	0.85	0.007	0.03	0.07	0.063	0.01	0.64	0.01	4.33

Table 2: Values of the parameters in Eqs. (11) and (12) for $D_s^+ \bar{D}^* \rightarrow K\psi(4040)$, $K\psi(4160)$, and $K\psi(4415)$. a_1 and a_2 are in units of millibarns; b_1 , b_2 , d_0 , and $\sqrt{s_z}$ are in units of GeV; c_1 and c_2 are dimensionless.

final state	T/T_c	a_1	b_1	c_1	a_2	b_2	c_2	d_0	$\sqrt{s_z}$
$K\psi(4040)$	0	0.014	0.081	0.585	0.066	0.236	3.05	0.22	5.42
	0.65	0.059	0.001	0.12	0.502	0.017	0.91	0.015	4.34
	0.75	0.053	0.0001	0.03	0.905	0.0134	0.731	0.015	4.12
	0.85	0.042	0.0306	0.276	1.38	0.0244	2.07	0.025	3.82
	0.9	0.46	0.00058	0.57	2.38	0.0266	3.2	0.025	3.67
	0.95	1.55	0.0009	0.48	1.14	0.0257	4.6	0.001	3.48
$K\psi(4160)$	0	0.022	0.04	0.54	0.044	0.18	2.24	0.15	5.53
	0.65	0.04	0.051	2.16	0.15	0.03	0.52	0.035	4.29
	0.75	0.11	0.014	0.49	0.14	0.044	1.53	0.035	4.09
	0.85	0.01	0.01	0.65	0.17	0.042	2.23	0.04	3.85
	0.9	0.005	0.001	1.02	0.129	0.047	3.33	0.045	3.7
	0.95	0.01	0.09	0.09	0.083	0.053	7.8	0.05	3.5
$K\psi(4415)$	0	0.0151	0.0658	0.561	0.0418	0.213	2.99	0.2	5.9
	0.65	0.114	0.012	0.54	0.053	0.197	5.19	0.015	4.58
	0.75	0.179	0.0119	0.56	0.056	0.164	4.8	0.015	4.31
	0.85	0.105	0.032	0.35	0.145	0.018	1.84	0.02	4.01

Table 3: The same as Table 1 except for $D_s^+ \bar{D}^* \rightarrow K^* \psi(4040)$, $K^* \psi(4160)$, and $K^* \psi(4415)$.

final state	T/T_c	a_1	b_1	c_1	a_2	b_2	c_2	d_0	$\sqrt{s_z}$
$K^* \psi(4040)$	0	0.04	0.02	0.46	0.068	0.1	0.96	0.06	5.78
	0.65	0.008	0.1	0.19	0.028	0.032	0.76	0.035	4.94
	0.75	0.002	0.041	0.1	0.027	0.029	0.6	0.03	4.73
	0.85	0.06	0.002	0.12	0.37	0.014	1.09	0.015	3.83
	0.9	0.18	0.003	0.47	0.5	0.04	2.79	0.04	3.63
	0.95	0.32	0.035	0.1	0.88	0.008	1.39	0.01	3.39
$K^* \psi(4160)$	0	0.009	0.016	0.41	0.024	0.08	0.66	0.05	5.89
	0.65	0.0002	0.028	0.04	0.0041	0.07	0.73	0.07	4.93
	0.75	0.001	0.0024	0.82	0.003	0.076	1.04	0.09	4.67
	0.85	0.007	0.0495	3.76	0.0275	0.0027	0.65	0.01	4.07
	0.9	0.015	0.0001	0.025	0.407	0.0073	0.609	0.01	3.63
	0.95	0.06	0.005	0.75	0.18	0.026	2.77	0.025	3.46
$K^* \psi(4415)$	0	0.01	0.04	0.71	0.02	0.08	0.43	0.05	6.2
	0.65	0.006	0.148	0.25	0.03	0.031	0.56	0.04	5.02
	0.75	0.0024	0.076	19.8	0.0235	0.0316	0.443	0.04	4.82
	0.85	0.052	0.003	0.3	0.207	0.017	1.17	0.015	3.93

Table 4: The same as Table 2 except for $D_s^{*+}\bar{D} \rightarrow K\psi(4040)$, $K\psi(4160)$, and $K\psi(4415)$.

final state	T/T_c	a_1	b_1	c_1	a_2	b_2	c_2	d_0	$\sqrt{s_z}$
$K\psi(4040)$	0	0.018	0.074	0.589	0.097	0.252	3.05	0.25	5.49
	0.65	0.08	0.003	0.34	0.9	0.031	1.38	0.03	4
	0.75	0.32	0.002	0.52	3.07	0.0249	1.59	0.03	4.16
	0.85	0.19	0.006	0.61	1.57	0.023	2.21	0.02	3.9
	0.9	0.118	0.0009	0.559	0.89	0.0242	4	0.025	3.69
	0.95	0.2	0.003	1.42	0.88	0.001	0.52	0.001	3.43
$K\psi(4160)$	0	0.033	0.044	0.54	0.062	0.189	2.35	0.17	5.48
	0.65	0.08	0.04	0.54	0.13	0.07	2.23	0.06	4.33
	0.75	0.04	0.017	0.64	0.23	0.067	2.55	0.065	4.13
	0.85	0.02	0.06	0.95	0.23	0.08	5.2	0.075	3.89
	0.9	0.15	0.073	18	0.069	0.0129	1.7	0.07	3.72
	0.95	0.062	0.066	18.1	0.189	0.0044	1.18	0.01	3.47
$K\psi(4415)$	0	0.02	0.072	0.554	0.059	0.228	2.96	0.22	5.86
	0.65	0.073	0.253	18	0.224	0.0142	0.78	0.025	4.6
	0.75	0.07	0.003	0.49	0.3	0.03	1.26	0.03	3.94
	0.85	0.078	0.009	0.27	0.301	0.05	5.6	0.05	4.03

Table 5: The same as Table 1 except for $D_s^{*+}\bar{D} \rightarrow K^*\psi(4040)$, $K^*\psi(4160)$, and $K^*\psi(4415)$.

final state	T/T_c	a_1	b_1	c_1	a_2	b_2	c_2	d_0	$\sqrt{s_z}$
$K^*\psi(4040)$	0	0.005	0.17	0.47	0.099	0.06	0.5	0.06	5.81
	0.65	0.003	0.026	0.03	0.05	0.034	0.57	0.04	4.93
	0.75	0.034	0.01	0.54	0.043	0.03	0.46	0.015	4.63
	0.85	0.2	0.03	0.33	0.41	0.04	4.79	0.04	3.85
	0.9	0.145	0.0001	0.05	2.63	0.0074	0.71	0.01	3.63
	0.95	0.128	0.0001	0.041	2.08	0.0085	0.63	0.01	3.4
$K^*\psi(4160)$	0	0.01	0.19	2.03	0.03	0.04	0.5	0.05	5.91
	0.65	0.001	0.044	0.33	0.004	0.108	1.12	0.1	4.98
	0.75	0.0049	0.0424	0.573	0.00193	0.175	4.08	0.04	4.68
	0.85	0.07	0.001	0.03	0.28	0.01	1.44	0.01	3.92
	0.9	0.03	0.003	0.19	0.25	0.02	1.67	0.02	3.73
	0.95	0.004	0.006	0.94	0.05	0.034	3.36	0.035	3.58
$K^*\psi(4415)$	0	0.018	0.13	0.8	0.021	0.03	0.48	0.05	6.3
	0.65	0.004	0.008	0.35	0.053	0.037	0.51	0.04	5.01
	0.75	0.016	0.011	0.84	0.045	0.027	0.39	0.02	4.74
	0.85	0.07	0.007	0.79	0.33	0.04	2.71	0.04	3.94

Table 6: The same as Table 2 except for $D_s^{*+} \bar{D}^* \rightarrow K\psi(4040)$, $K\psi(4160)$, and $K\psi(4415)$.

final state	T/T_c	a_1	b_1	c_1	a_2	b_2	c_2	d_0	$\sqrt{s_z}$
$K\psi(4040)$	0	0.011	0.053	0.56	0.031	0.321	5.24	0.31	5.51
	0.65	0.011	0.00112	0.54	0.233	0.0439	3.73	0.04	4.43
	0.75	0.01	0.014	0.87	0.26	0.03	2.26	0.03	4.23
	0.85	0.016	0.059	0.4	0.063	0.024	3.6	0.02	3.94
	0.9	0.037	0.003	1	0.099	0.001	0.499	0.001	3.67
	0.95	0.128	0.03	15	0.79	0.00135	0.75	0.001	3.36
$K\psi(4160)$	0	0.002	0.006	0.395	0.027	0.148	1.19	0.19	5.59
	0.65	0.0015	0.008	0.55	0.0849	0.109	6.1	0.1	4.67
	0.75	0.0008	0.0054	0.496	0.0679	0.0852	5.3	0.08	4.47
	0.85	0.0062	0.097	1.66	0.0027	0.0089	0.962	0.07	4.21
	0.9	0.0024	0.025	0.46	0.063	0.013	2.92	0.01	3.8
	0.95	0.002	0.0008	0.142	0.078	0.0125	3.55	0.01	3.41
$K\psi(4415)$	0	0.0027	0.055	0.59	0.0218	0.24	2.8	0.24	5.94
	0.65	0.044	0.0052	0.625	0.223	0.088	10.5	0.09	4.54
	0.75	0.195	0.0727	8.79	0.0156	0.00282	0.603	0.07	4.34
	0.85	0.052	0.001	1.27	0.111	0.002	0.32	0.001	3.98

Table 7: The same as Table 1 except for $D_s^{*+}\bar{D}^* \rightarrow K^*\psi(4040)$, $K^*\psi(4160)$, and $K^*\psi(4415)$.

final state	T/T_c	a_1	b_1	c_1	a_2	b_2	c_2	d_0	$\sqrt{s_z}$
$K^*\psi(4040)$	0	0.051	0.015	0.43	0.138	0.09	0.93	0.07	5.71
	0.65	0.0001	0.002	0.002	0.305	0.021	0.5	0.02	4.63
	0.75	0.05	0.002	0.29	0.7	0.028	1.27	0.03	4.19
	0.85	0.49	0.03	0.04	2.53	0.01	1.57	0.01	3.83
	0.9	0.01	0.001	0.01	3.24	0.007	0.48	0.01	3.62
	0.95	0.16	0.02	0.95	2.98	0.006	0.43	0.01	3.37
$K^*\psi(4160)$	0	0.01	0.03	0.47	0.05	0.06	0.5	0.05	5.81
	0.65	0.0056	0.003	0.51	0.0178	0.108	1.7	0.1	4.84
	0.75	0.025	0.096	3.74	0.094	0.0042	0.57	0.01	4.46
	0.85	0.041	0.001	0.05	0.361	0.016	1.51	0.015	3.96
	0.9	0.014	0.012	0.71	0.037	0.031	3.72	0.03	3.84
	0.95	0.00234	0.22	0.23	0.00522	0.0336	3.79	0.04	3.67
$K^*\psi(4415)$	0	0.01	0.11	0.63	0.05	0.05	0.49	0.05	6.13
	0.65	0.04	0.04	0.2	0.19	0.023	0.67	0.02	4.75
	0.75	0.12	0.008	0.48	0.37	0.034	1.61	0.03	4.3
	0.85	0.25	0.065	6.2	0.42	0.009	0.59	0.01	3.95

Table 8: The same as Table 2 except for $D_s^+ D_s^{*-} \rightarrow \eta\psi(4040)$, $\eta\psi(4160)$, and $\eta\psi(4415)$.

final state	T/T_c	a_1	b_1	c_1	a_2	b_2	c_2	d_0	$\sqrt{s_z}$
$\eta\psi(4040)$	0	0.009	0.113	0.59	0.037	0.285	4.7	0.31	5.46
	0.65	0.14	0.009	0.55	0.8	0.037	1.66	0.03	4.44
	0.75	0.3	0.011	0.53	0.54	0.03	1.73	0.03	4.29
	0.85	0.19	0.009	0.53	0.23	0.023	1.61	0.01	4.07
	0.9	0.032	0.099	0.25	0.109	0.014	0.93	0.01	3.9
	0.95	0.03	0.04	0.6	0.022	0.012	2.82	0.02	3.75
$\eta\psi(4160)$	0	0.012	0.053	0.54	0.024	0.205	2.71	0.19	5.62
	0.65	0.03	0.057	0.58	0.07	0.078	2.69	0.075	4.48
	0.75	0.0014	0.057	0.55	0.19	0.088	3.33	0.09	4.26
	0.85	0.001	0.23	0.44	0.064	0.068	3.9	0.05	4.19
	0.9	0.00023	0.0024	0.57	0.0278	0.0551	5.04	0.05	3.86
	0.95	0.00028	0.0044	0.695	0.0162	0.0529	7.1	0.05	3.62
$\eta\psi(4415)$	0	0.0053	0.065	0.58	0.0242	0.24	3.28	0.27	5.86
	0.65	0.038	0.271	21.3	0.117	0.0188	0.7	0.035	4.64
	0.75	0.07	0.026	0.26	0.15	0.055	3.68	0.05	4.41
	0.85	0.08	0.022	0.55	0.17	0.047	3.69	0.05	4.17

Table 9: The same as Table 2 except for $D_s^{*+}D_s^{*-} \rightarrow \eta\psi(4040)$, $\eta\psi(4160)$, and $\eta\psi(4415)$.

final state	T/T_c	a_1	b_1	c_1	a_2	b_2	c_2	d_0	$\sqrt{s_z}$
$\eta\psi(4040)$	0	0.0097	0.042	0.58	0.0197	0.365	7.7	0.37	5.5
	0.65	0.016	0.245	16.1	0.0343	0.026	1.33	0.03	4.63
	0.75	0.055	0.0154	0.81	0.025	0.201	27	0.03	4.45
	0.85	0.0118	0.011	0.69	0.0064	0.16	6.9	0.01	4.42
	0.9	0.00076	0.026	0.75	0.00145	0.139	3.9	0.1	4.42
	0.95	0.0007	0.004	0.39	0.0009	0.083	1.58	0.1	4.21
$\eta\psi(4160)$	0	0.005	0.1	0.55	0.0105	0.229	3.25	0.22	5.64
	0.65	0.0046	0.842	0.496	0.0259	0.103	4.15	0.1	4.86
	0.75	0.003	0.147	0.52	0.018	0.079	3.46	0.07	4.71
	0.85	0.002	0.128	0.56	0.003	0.075	3.24	0.05	4.52
	0.9	0.0003	0.4	0.5	0.0009	0.106	1.9	0.1	4.33
	0.95	0.00002	0.002	0.33	0.000475	0.132	1.3	0.15	4.08
$\eta\psi(4415)$	0	0.002	0.14	0.61	0.0101	0.29	4.26	0.33	5.92
	0.65	0.042	0.08	11.7	0.03	0.31	15.9	0.08	4.77
	0.75	0.025	0.275	18.9	0.032	0.059	7.4	0.06	4.6
	0.85	0.0052	0.227	13.3	0.0033	0.036	0.82	0.04	4.64

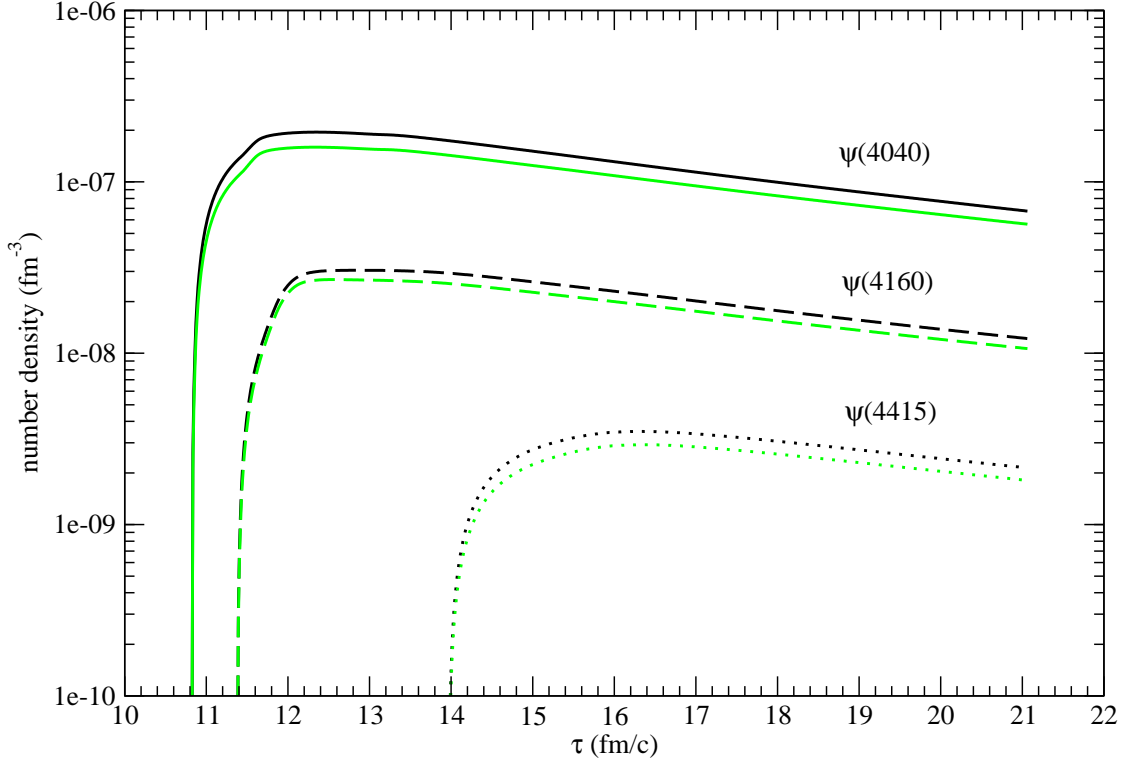


Figure 28: Number densities as functions of τ at $r = 0$ fm. The upper solid, upper dashed, and upper dotted curves result from reactions between two open-charm mesons and their reverse reactions, and the lower solid, lower dashed, and lower dotted curves from reactions between two charmed mesons and their reverse reactions.

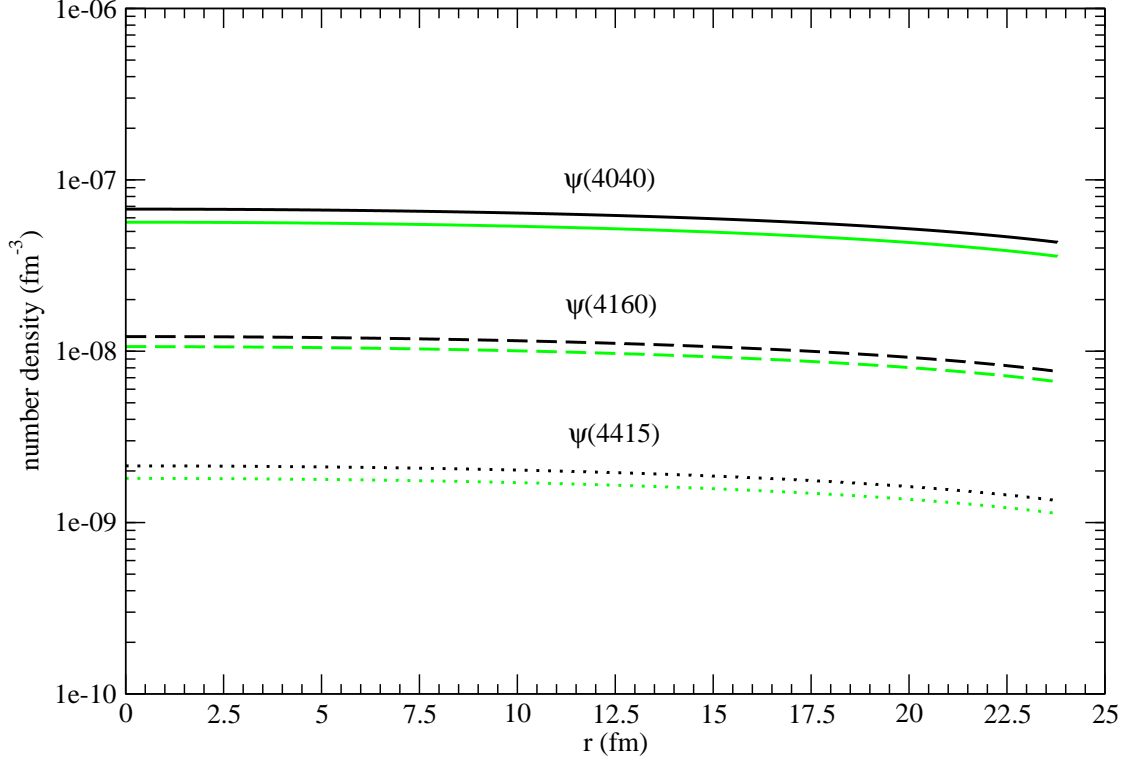


Figure 29: The same as Fig. 28, but for r dependence at kinetic freeze-out.

The potential given in Eq. (10) shows explicit dependence on temperature. The Schrödinger equation with the potential gives temperature dependence of meson masses and mesonic quark-antiquark relative-motion wave functions. Since $\sqrt{s_0}$, \sqrt{s} , $|\vec{P}|$, and $|\vec{P}'|$ relate to the meson masses, they depend on temperature. Consequently, the cross sections for the production of $\psi(4040)$, $\psi(4160)$, and $\psi(4415)$ mesons depend on temperature as seen in Figs. 1-27. When hadronic matter expands, contributions of the twenty-seven reactions to charmonium production differ at different temperatures. This may also be understood from the maximum of the five peak cross sections of an endothermic reaction, which correspond to the temperatures $0.65T_c$, $0.75T_c$, $0.85T_c$, $0.9T_c$, and $0.95T_c$. For example, the largest peak cross section of $D_s^+\bar{D} \rightarrow K^*\psi(4160)$ ($D_s^+\bar{D}^* \rightarrow K\psi(4160)$, $D_s^+\bar{D}^* \rightarrow K^*\psi(4160)$, $D_s^{*+}\bar{D} \rightarrow K\psi(4160)$, $D_s^{*+}\bar{D}^* \rightarrow K^*\psi(4160)$) appears at the temperature $0.95T_c$ ($0.75T_c$, $0.9T_c$, $0.85T_c$, $0.85T_c$). The endothermic reaction $D_s^+\bar{D} \rightarrow K^*\psi(4160)$ ($D_s^+\bar{D}^* \rightarrow K\psi(4160)$, $D_s^+\bar{D}^* \rightarrow K^*\psi(4160)$, $D_s^{*+}\bar{D} \rightarrow K\psi(4160)$, $D_s^{*+}\bar{D}^* \rightarrow K^*\psi(4160)$) may thus produce the largest amount of $\psi(4160)$ mesons at $0.95T_c$.

$(0.75T_c, 0.9T_c, 0.85T_c, 0.85T_c)$ during evolution of hadronic matter.

Temperature dependence of the interquark potential has been obtained in the lattice gauge calculations. It is shown from the potential that the interaction range drops sharply around the critical temperature [49]. Consequently, the $c\bar{c}$ relative-motion wave functions obtained from the Schrödinger equation with the potential exhibit that the spatial size of each wave function increases rapidly from a temperature. This temperature is near the critical temperature, and has different values for different quantum numbers of $c\bar{c}$ states. We thus take this temperature as the dissociation temperature of the $c\bar{c}$ state. This way is valid not only for bound states like J/ψ , χ_c , and ψ' but also for resonances like $\psi(4040)$, $\psi(4160)$, and $\psi(4415)$.

Number densities obtained from the master rate equations depend on the average cross sections weighted by the relative velocity and the dissociation temperatures of $\psi(4040)$, $\psi(4160)$, and $\psi(4415)$ mesons. The averages $\langle\sigma_{ij\rightarrow i'\psi(4040)}v_{ij}\rangle$ and $\langle\sigma_{ij\rightarrow i'\psi(4415)}v_{ij}\rangle$ are typically 5 and 3.3 times $\langle\sigma_{ij\rightarrow i'\psi(4160)}v_{ij}\rangle$, respectively. In addition, the $\psi(4040)$ dissociation temperature is higher than the $\psi(4160)$ dissociation temperature. Hadronic matter has a longer time to produce $\psi(4040)$ than to produce $\psi(4160)$. We thus see that the $\psi(4040)$ number density is larger than the $\psi(4160)$ number density in Figs. 28 and 29. However, because the $\psi(4415)$ dissociation temperature is lower than the $\psi(4160)$ dissociation temperature, hadronic matter has a shorter time to produce $\psi(4415)$ than to produce $\psi(4160)$. This factor causes the $\psi(4415)$ number density smaller than the $\psi(4160)$ number density. The number densities and the volume of hadronic matter at kinetic freeze-out give 0.0034, 0.0006, and 0.00011 as the numbers of $\psi(4040)$, $\psi(4160)$, and $\psi(4415)$ mesons produced in a central Pb-Pb collision at $\sqrt{s_{NN}} = 5.02$ TeV, respectively.

The first twenty-four terms on the right-hand side of Eq. (2) are gain terms of producing $\psi(4040)$, $\psi(4160)$, and $\psi(4415)$ mesons, and the other terms are loss terms of breaking the three mesons. The cross sections for $q_1\bar{q}_2 + c\bar{c} \rightarrow c\bar{q}_2 + q_1\bar{c}$ in the loss terms are obtained from those for $c\bar{q}_2 + q_1\bar{c} \rightarrow q_1\bar{q}_2 + c\bar{c}$ by the detailed balance. The difference between the number densities obtained from Eq. (1) with the loss terms and without the loss terms is small. For example, the $\psi(4040)$ ($\psi(4160)$, $\psi(4415)$) number density at $r = 0$

fm and at kinetic freeze-out is $6.75 \times 10^{-8} \text{ fm}^{-3}$ ($1.22 \times 10^{-8} \text{ fm}^{-3}$, $2.14 \times 10^{-9} \text{ fm}^{-3}$) with the loss terms and $7.35 \times 10^{-8} \text{ fm}^{-3}$ ($1.25 \times 10^{-8} \text{ fm}^{-3}$, $2.21 \times 10^{-9} \text{ fm}^{-3}$) without the loss terms. The reason of the small difference is that the number densities of the three mesons are small.

V. SUMMARY

We have studied the production of $\psi(4040)$, $\psi(4160)$, and $\psi(4415)$ mesons in ultra-relativistic heavy-ion collisions at the LHC. This research includes two parts. In one part we have studied the charmonium production from the reactions between charmed strange mesons and open-charm mesons. Fifty-one reactions are considered, and we have presented numerical unpolarized cross sections and their parametrizations for the twenty-seven reactions: $D_s^+ \bar{D} \rightarrow K^* R$, $D_s^+ \bar{D}^* \rightarrow KR$, $D_s^+ \bar{D}^* \rightarrow K^* R$, $D_s^{*+} \bar{D} \rightarrow KR$, $D_s^{*+} \bar{D} \rightarrow K^* R$, $D_s^{*+} \bar{D}^* \rightarrow KR$, $D_s^{*+} \bar{D}^* \rightarrow K^* R$, $D_s^+ D_s^{*-} \rightarrow \eta R$, and $D_s^{*+} D_s^{*-} \rightarrow \eta R$, where R indicates $\psi(4040)$, $\psi(4160)$, or $\psi(4415)$. In another part we have studied the production of $\psi(4040)$, $\psi(4160)$, and $\psi(4415)$ in hadronic matter that results from the quark-gluon plasma created in Pb-Pb collisions at the LHC. We have established the master rate equations with the new source terms that include the reactions between charmed strange mesons and open-charm mesons and their reverse reactions. Temperature dependence of the cross sections reflects different contributions of the fifty-one reactions to the charmonium production at different temperatures. The master rate equations in association with the hydrodynamic equation are solved to obtain number densities of $\psi(4040)$, $\psi(4160)$, and $\psi(4415)$. In central Pb-Pb collisions at $\sqrt{s_{NN}} = 5.02 \text{ TeV}$ the $\psi(4040)$ number density is larger than the $\psi(4160)$ number density, and the latter is larger than the $\psi(4415)$ number density.

ACKNOWLEDGEMENTS

This work was supported by the project STRONG-2020 of European Center for Theoretical Studies in Nuclear Physics and Related Areas.

References

- [1] J.-E. Augustin *et al.*, Phys. Rev. Lett. 34, 764 (1975).
- [2] J. Siegrist *et al.*, Phys. Rev. Lett. 36, 700 (1976).
- [3] R. Brandelik *et al.*, Phys. Lett. 76 B, 361 (1978).
- [4] V. Zhukova *et al.*, Phys. Rev. D 97, 012002 (2018).
- [5] M. Ablikim *et al.*, Phys. Rev. D 101, 012008 (2020).
- [6] R. Aaij *et al.*, Phys. Rev. D 102, 112003 (2020).
- [7] M. Ablikim *et al.*, Phys. Rev. D 102, 112009 (2020).
- [8] M. Ablikim *et al.*, Phys. Rev. D 104, 092001 (2021).
- [9] M. Ablikim *et al.*, Phys. Rev. D 104, 112009 (2021).
- [10] M. Ablikim *et al.*, J. High Energy Phys. 07, 064 (2022).
- [11] L.-K. Hao, K.-Y. Liu, and K.-T. Chao, Phys. Lett. B 546, 216 (2002).
- [12] M. Piotrowska, F. Giacosa, and P. Kovacs, Eur. Phys. J. C 79, 98 (2019).
- [13] M. Bayar, N. Ikeno, and E. Oset, Eur. Phys. J. C 80, 222 (2020).
- [14] S. Godfrey and N. Isgur, Phys. Rev. D 32, 189 (1985).
- [15] T. Barnes, S. Godfrey, and E. S. Swanson, Phys. Rev. D 72, 054026 (2005).
- [16] J. Vijande, F. Fernández, and A. Valcarce, J. Phys. G 31, 481 (2005).
- [17] P. G. Ortega, J. Segovia, D. R. Entem, and F. Fernández, Phys. Lett. B 778, 1 (2018).
- [18] W.-X. Li, X.-M. Xu, and H. J. Weber, Eur. Phys. J. C 81, 225 (2021).
- [19] L.-Y. Li, X.-M. Xu, and H. J. Weber, Phys. Rev. D 105, 114025 (2022).

- [20] H. von Gersdorff, L. McLerran, M. Kataja, and P. V. Ruuskanen, *Phys. Rev. D* 34, 794 (1986).
- [21] P. F. Kolb and U. Heinz, arXiv:nucl-th/0305084.
- [22] H. Niemi, K. J. Eskola, and R. Paatelainen, *Phys. Rev. C* 93, 024907 (2016).
- [23] T. Barnes and E. S. Swanson, *Phys. Rev. D* 46, 131 (1992).
- [24] E. S. Swanson, *Ann. Phys. (N.Y.)* 220, 73 (1992).
- [25] N. F. Mott and H. S. W. Massey, *The theory of Atomic Collisions* (Clarendon, Oxford, 1965).
- [26] T. Barnes, N. Black, and E. S. Swanson, *Phys. Rev. C* 63, 025204 (2001).
- [27] C.-Y. Wong and H. W. Crater, *Phys. Rev. C* 63, 044907 (2001).
- [28] W. Buchmüller and S.-H. H. Tye, *Phys. Rev. D* 24, 132 (1981).
- [29] F. Karsch, E. Laermann, and A. Peikert, *Nucl. Phys. B* 605, 579 (2001).
- [30] X.-M. Xu, *Nucl. Phys. A* 697, 825 (2002).
- [31] M. Tanabashi *et al.* (Particle Data Group), *Phys. Rev. D* 98, 030001 (2018) and 2019 update.
- [32] E. Colton, E. Malamud, P. E. Schlein, A. D. Johnson, V. J. Stenger, and P. G. Wohlmut, *Phys. Rev. D* 3, 2028 (1971).
- [33] N. B. Durusoy, M. Baubillier, R. George, M. Goldberg, A. M. Touchard, N. Armenise, M. T. Fogli-Muciaccia, and A. Silvestri, *Phys. Lett. B* 45, 517 (1973).
- [34] M. J. Losty, V. Chaloupka, A. Ferrando, L. Montanet, E. Paul, D. Yaffe, A. Zieminski, J. Alitti, B. Gandois, and J. Louie, *Nucl. Phys. B* 69, 185 (1974).
- [35] W. Hoogland *et al.*, *Nucl. Phys. B* 126, 109 (1977).

- [36] S. D. Protopopescu, M. Alston-Garnjost, A. Barbaro-Galtieri, S. M. Flatté, J. H. Friedman, T. A. Lasinski, G. R. Lynch, M. S. Rabin, and F. T. Solmitz, *Phys. Rev. D* 7, 1279 (1973).
- [37] B. Hyams *et al.*, *Nucl. Phys. B* 64, 134 (1973).
- [38] P. Estabrooks and A. D. Martin, *Nucl. Phys. B* 79, 301 (1974).
- [39] V. Srinivasan *et al.*, *Phys. Rev. D* 12, 681 (1975).
- [40] L. Rosselet *et al.*, *Phys. Rev. D* 15, 574 (1977).
- [41] C. D. Froggatt and J. L. Petersen, *Nucl. Phys. B* 129, 89 (1977).
- [42] A. A. Bel'kov, S. A. Bunyatov, K. N. Mukhin, O. O. Patarakin, V. M. Sidorov, M. M. Sulkovskaya, A. F. Sustavov, and V. A. Yarba, *JETP Lett.* 29, 597 (1979).
- [43] E. A. Alekseeva, A. A. Kartamyshev, V. K. Makar'in, K. N. Mukhin, O. O. Patarakin, M. M. Sulkovskaya, A. F. Sustavov, L. V. Surkova, and L. A. Chernysheva, *Sov. Phys. JETP* 55, 591 (1982).
- [44] R. García-Martín, R. Kamiński, J. R. Peláez, J. R. de Elvira, and F. J. Ynduráin, *Phys. Rev. D* 83, 074004 (2011).
- [45] J. Zhou and X.-M. Xu, *Phys. Rev. C* 85, 064904 (2012).
- [46] Z.-Y. Shen, X.-M. Xu, and H. J. Weber, *Phys. Rev. D* 94, 034030 (2016).
- [47] Y.-P. Zhang, X.-M. Xu, and H.-J. Ge, *Nucl. Phys. A* 832, 112 (2010).
- [48] X.-M. Xu, C.-C. Ma, A.-Q. Chen, and H. J. Weber, *Phys. Lett. B* 645, 146 (2007).
- [49] H. Satz, arXiv:hep-ph/0602245.
- [50] S. Acharya *et al.*, *J. High Energy Phys.* 10, 174 (2018).
- [51] F. Cooper and G. Frye, *Phys. Rev. D* 10, 186 (1974).

[52] S. Acharya *et al.*, Phys. Rev. C 101, 044907 (2020).

[53] S. Acharya *et al.*, Phys. Rev. C 106, 034907 (2022).